Nucleolar accumulation of APE1 depends on charged lysine residues that undergo acetylation upon genotoxic stress and modulate its BER activity in cells

Lisa Lirussi[a,*], Giulia Antoniali[a,*], Carlo Vascotto[a], Chiara D'Ambrosio[b], Mattia Poletto[a], Milena Romanello[a], Daniela Marasco[c,d], Marilisa Leone[d], Franco Quadrifoglio[a], Kishor K. Bhakat[e], Andrea Scaloni[b], and Gianluca Tell[a]

[a]Department of Medical and Biological Sciences, University of Udine, 33100 Udine, Italy; [b]Proteomics and Mass Spectrometry Laboratory, Istituto di Ricerche per il Sistema Produzione Animale in Ambiente Mediterraneo, National Research Council, 80147 Naples, Italy; [c]Department of Biological Sciences, University of Naples "Federico II," 80134 Naples, Italy; [d]Institute of Biostructures and Bioimaging, National Research Council, 80134 Naples, Italy; [e]Department of Biochemistry and Molecular Biology, University of Texas Medical Branch, Galveston, TX 77555

ABSTRACT **Apurinic/apyrimidinic endonuclease 1 (APE1) is the main abasic endonuclease in the base excision repair (BER) pathway of DNA lesions caused by oxidation/alkylation in mammalian cells; within nucleoli it interacts with nucleophosmin and rRNA through N-terminal Lys residues, some of which ($K^{27}/K^{31}/K^{32}/K^{35}$) may undergo acetylation in vivo. Here we study the functional role of these modifications during genotoxic damage and their in vivo relevance. We demonstrate that cells expressing a specific K-to-A multiple mutant are APE1 nucleolar deficient and are more resistant to genotoxic treatment than those expressing the wild type, although they show impaired proliferation. Of interest, we find that genotoxic treatment induces acetylation at these K residues. We also find that the charged status of $K^{27}/K^{31}/K^{32}/K^{35}$ modulates acetylation at K^{6}/K^{7} residues that are known to be involved in the coordination of BER activity through a mechanism regulated by the sirtuin 1 deacetylase. Of note, structural studies show that acetylation at $K^{27}/K^{31}/K^{32}/K^{35}$ may account for local conformational changes on APE1 protein structure. These results highlight the emerging role of acetylation of critical Lys residues in regulating APE1 functions. They also suggest the existence of cross-talk between different Lys residues of APE1 occurring upon genotoxic damage, which may modulate APE1 subnuclear distribution and enzymatic activity in vivo.**

Monitoring Editor
Karsten Weis
University of California, Berkeley

Received: Apr 17, 2012
Revised: Jul 25, 2012
Accepted: Aug 16, 2012

This article was published online ahead of print in MBoC in Press (http://www.molbiolcell.org/cgi/doi/10.1091/mbc.E12-04-0299) on August 23, 2012.

*These authors contributed equally to this work

The authors declare that they have no conflict of interests.

Address correspondence to: Gianluca Tell (gianluca.tell@uniud.it).

Abbreviations used: APE1/Ref-1, apurinic/apyrimidinic endonuclease/redox effector factor 1; BER, base excision repair; MMS, methyl methanesulfonate; MTS, 3-(4-5-dimethylthiazol-2-yl)-5-(3-carboxymethoxyphenyl)-2-(4-sulfophenyl)-2H-tetrazolium salt; NPM1, nucleophosmin 1; SIRT1, sirtuin 1; TBHP, *tert*-butyl hydroperoxide.

INTRODUCTION

Apurinic/apyrimidinic endonuclease 1/redox effector factor-1 (APE1) plays a central role in the maintenance of genome stability and redox signaling (Bapat *et al.*, 2009, 2010; Tell *et al.*, 2010a; Wilson and Simeonov, 2010). Through its C-terminal domain (residues 61–318), it acts as an essential enzyme in the base excision repair (BER) pathway of DNA damages caused by both endogenous and exogenous oxidizing/alkylating agents, including many chemotherapeutic drugs. In combination with thioredoxin (Ueno *et al.*, 1999; Seemann and Hainaut, 2005) and through its N-terminal domain (residues 1–127), it also functions as a regulatory redox agent to maintain cancer-related transcription factors (Egr-1, NF-κB, p53, HIF-1α, AP-1, and Pax proteins) in an active reduced state (Hirota *et al.*, 1997;

Wei *et al.*, 2000; Ziel *et al.*, 2004; Gray *et al.*, 2005; Pines *et al.*, 2005; Tell *et al.*, 2005, 2010a). APE1 can also act as a transcriptional repressor through indirect binding to negative Ca^{2+}-response elements (nCaRE), which are regulated by K^6/K^7 acetylation (Bhakat *et al.*, 2003). Recently APE1 was demonstrated to bind/cleave abasic RNA (Vascotto *et al.*, 2009b; Fantini *et al.*, 2010; Tell *et al.*, 2010b) and to control *c-Myc* expression by cleaving its mRNA (Barnes *et al.*, 2009). These discoveries pointed to a new function of APE1 in regulating gene expression through posttranscriptional mechanisms and brought to light the fact that this protein is a possible target for anticancer therapy.

In this context, we showed that the first 35 amino acids in the nonstructured N-terminal domain of APE1 are required for a stable interaction with rRNA, nucleophosmin 1 (NPM1), and other proteins involved in ribosome biogenesis/RNA processing (Vascotto *et al.*, 2009b; Tell *et al.*, 2010b). In particular, K residues within the protein region spanning amino acids 24–35 are involved in the interaction of APE1 with both rRNA and NPM1 and also regulate its in vitro enzymatic activity (Fantini *et al.*, 2010). Of interest, some of these critical K residues, namely $K^{27}/K^{31}/K^{32}/K^{35}$, undergo in vivo acetylation. These results suggest that protein–protein interactions and/or posttranslational modifications (PTMs) involving the APE1 N-terminal domain may play important roles in vivo in coordinating and fine-tuning the protein's BER activity and functions on rRNA metabolism. Recently it was also demonstrated that APE1 K^6/K^7 may undergo acetylation during cell response to genotoxic treatment (Fantini *et al.*, 2008) and that the acetylation status of these K residues, controlled by the sirtuin 1 (SIRT1) deacetylase activity, should be important in modulating protein DNA-repair function by regulating the kinetics of its interaction with other enzymes involved in BER, for example, XRCC1 (Yamamori *et al.*, 2010).

APE1 is mainly a nuclear protein and is critical for controlling cellular proliferative rates (Fung and Demple, 2005; Izumi *et al.*, 2005; Vascotto *et al.*, 2009b). We also showed that a considerable amount of APE1 is accumulated within the nucleoli of different cell lines (Vascotto *et al.*, 2009b; Fantini *et al.*, 2010), but its role within this compartment is unknown. Cytoplasmic, mitochondrial, and endoplasmic reticulum localizations have also been ascertained (Tell *et al.*, 2001; Szczesny and Mitra, 2005; Chattopadhyay *et al.*, 2006; Grillo *et al.*, 2006; Mitra *et al.*, 2007). APE1 is an abundant and relatively stable protein in mammalian cells (Tell *et al.*, 2009, 2010a). Fine-tuning of the multiple APE1 functions may therefore depend on the modulation of its PTMs and, eventually, on its interactome. Although a functional role has been determined for some PTMs (K^6/K^7 acetylation and $K^{24}/K^{25}/K^{27}$ ubiquitination; Bhakat *et al.*, 2003; Fantini *et al.*, 2008; Busso *et al.*, 2009), the identity and importance of various interacting partners in modulating APE1 biological functions are still under investigation (Parlanti *et al.*, 2007; Busso *et al.*, 2009; Vascotto *et al.*, 2009b). APE1 may affect cell growth by directly acting on rRNA quality control mechanisms; in particular, APE1 interaction with NPM1 may affect its activity over rRNA molecules. However, many aspects of this new function are undefined (Vascotto *et al.*, 2009b; Tell *et al.*, 2010b).

In this study, we address the biological role of APE1 acetylation at $K^{27}/K^{31}/K^{32}/K^{35}$ and, in light of recent evidence showing the emerging function of the nucleolus as a central sensor of protein trafficking during DNA repair after genotoxic treatment (Nalabothula *et al.*, 2010), the role of the nucleolus itself on the APE1 protective function toward genotoxic damage. We used a reconstitution strategy with APE1 mutants in which the charged Lys residues were replaced by either Ala or Arg to mimic constitutive acetylated ($APE1^{K4pleA}$) and nonacetylatable ($APE1^{K4pleR}$) protein forms, respectively. These mutants are reintroduced into APE1-silenced cell clones to determine the role of these crucial amino acids during cell response to genotoxic treatment.

RESULTS

Positively charged $K^{27}/K^{31}/K^{32}/K^{35}$ residues are essential for APE1 nucleolar accumulation through stabilization of protein interaction with NPM1 and rRNA

We previously demonstrated that charged K residues, located within the unstructured APE1 N-terminal domain (i.e., $K^{24}/K^{25}/K^{27}/K^{31}/K^{32}$), are crucial for APE1 interaction with rRNA and NPM1 and for modulating its catalytic activity on abasic DNA through regulation of product binding. Of interest, some of these critical amino acids (i.e., $K^{27}/K^{31}/K^{32}$ in addition to K^{35}) may undergo in vivo acetylation under basal conditions (Fantini *et al.*, 2010). We hypothesized that the degree of positive charges, modified by acetylation at these residues, may modulate APE1's different functions through its redirection to different substrates and/or stimulation of its DNA-repair enzymatic activity (Fantini *et al.*, 2010). To address this issue, we inspected the role of the positively charged residues within the region 27–35 in modulating the interaction between APE1 and NPM1. Colocalization experiments in HeLa cells transiently transfected with either FLAG-tagged, wild-type APE1 ($APE1^{WT}$), a K-to-A mutant ($APE1^{K4pleA}$) in which the positive charges have been removed as in the case of constitutive acetylation, or a nonacetylatable K-to-R APE1 mutant ($APE1^{K4pleR}$) showed that $APE1^{K4pleA}$ mutant has a marked exclusion from the nucleoli apparent in all expressing cells (Figure 1A). Silencing of the endogenous APE1 protein did not alter either the ability of the $APE1^{WT}$ and $APE1^{K4pleR}$ proteins to accumulate within the nucleolar compartment or the inability of the $APE1^{K4pleA}$ to accumulate within the nucleolus (unpublished data). These data thus demonstrate that $APE1^{WT}$ and $APE1^{K4pleR}$ nucleolar accumulation is not the consequence of their overexpression.

To complement these observations and also to exclude a possible contribution of the FLAG tag used to generate recombinant ectopic proteins, we exploited a live-cell imaging system as suggested by Schnell *et al.* (2012). APE1 cDNA was cloned into a pDendra2 vector to express APE1 in fusion with the green photoconvertible fluorophore Dendra (Chudakov *et al.*, 2007). As reported in Figure 1B, the fluorophore alone is present in both the cytoplasm and the nuclear compartment, but it is completely excluded from the nucleoli, as demonstrated by quantitative fluorescence signal analyses. In contrast, whereas the expression of Dendra in fusion with $APE1^{WT}$ and $APE1^{K4pleR}$ results in an efficient accumulation of the protein within the nucleolar compartment, the Dendra-$APE1^{K4pleA}$ mutant displays a homogeneous nuclear distribution. This approach confirms immunofluorescence-based data on the reduced accumulation of FLAG-tagged $APE1^{K4pleA}$ within the nucleoli and supports the evidence that the nucleolar accumulation of APE1 protein does not depend on the protein abundance nor does it depend on the specific tag used to generate the ectopic recombinant proteins (see also Supplemental Figure S1).

We supported our immunofluorescence data with biochemical interaction experiments. Coimmunoprecipitation analysis showed that the $APE1^{K4pleA}$ mutant has a significantly reduced interaction with NPM1 (Figure 2A), in accordance with its impaired nucleolar accumulation. The altered electrophoretic mobility observed for the $APE1^{K4pleA}$ mutant (Figure 2A) was further confirmed by SDS–PAGE analysis of recombinant proteins expressed in *Escherichia coli* and purified by chromatography. The effect is likely due to alteration of its overall charge, since electrospray ionization mass spectrometry analysis confirmed the correctness of protein mass values, and the

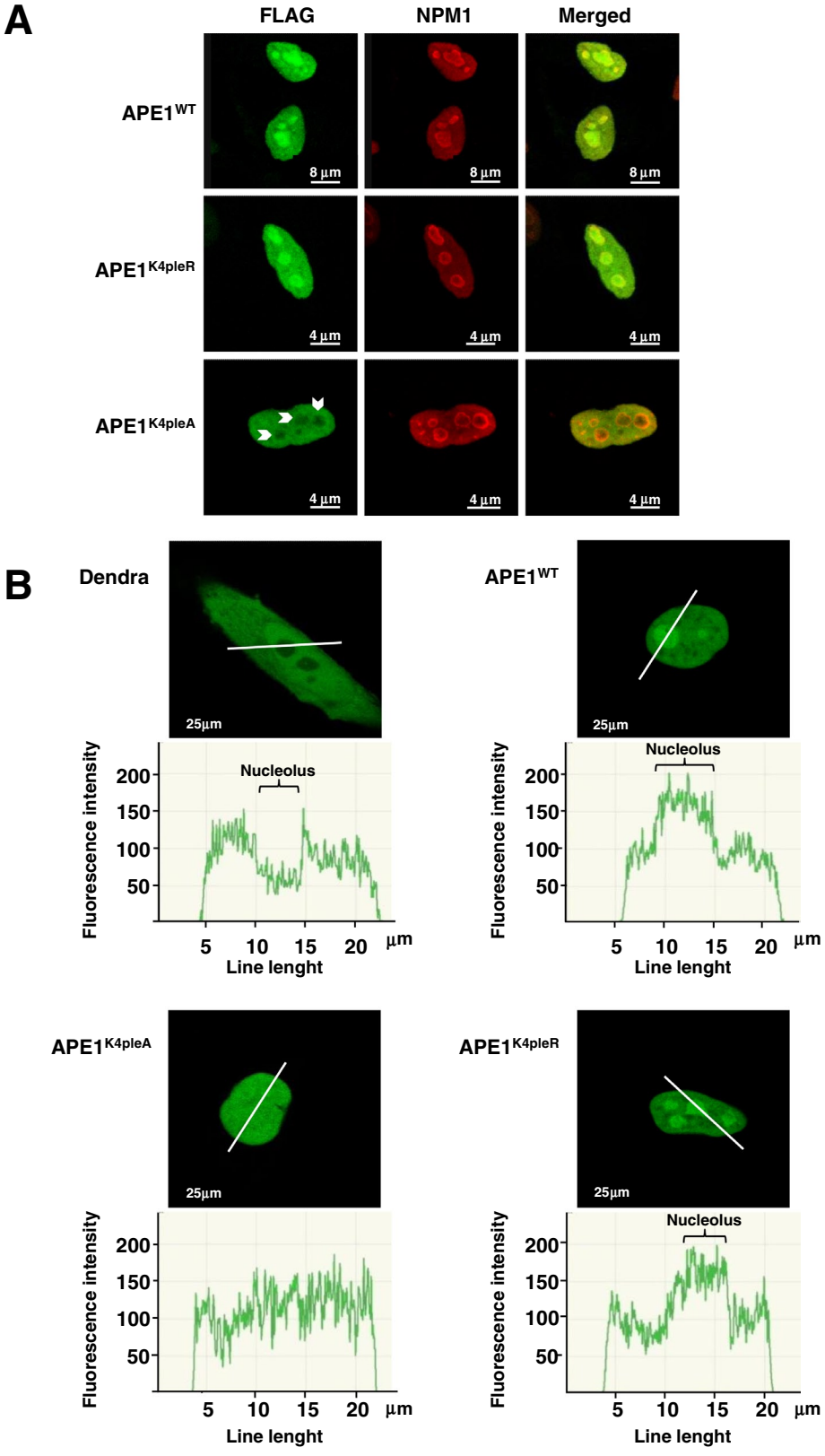

FIGURE 1: Positively charged $K^{27}/K^{31}/K^{32}/K^{35}$ residues are required for APE1 nucleolar accumulation. (A) Confocal microscopy of HeLa cells transfected with $APE1^{WT}$, $APE1^{K4pleA}$, or $APE1^{K4pleR}$ FLAG-tagged proteins and stained with antibodies against NPM1 (red) and ectopic FLAG-APE1 (green). Overlap of staining (yellow) demonstrated colocalization of the two proteins. Of note, the $APE1^{K4pleA}$ mutant was completely excluded from nucleoli (white arrowheads), whereas both $APE1^{WT}$ and the $APE1^{K4pleR}$ were accumulated within. Images are representative of 100% of transfected cells. (B) HeLa cells transfected with pDendra2-N empty vector or encoding APE1 (wild-type and mutants) in fusion with Dendra fluorophore were analyzed with a live confocal microscopy workstation. Cells transfected with empty vector (Dendra) showed diffuse green fluorescence within cytoplasm and nucleus, with exclusion of the nucleolar compartment. $APE1^{WT}$ and $APE1^{K4pleR}$ mutant mainly localized within the nuclear compartment and accumulated within nucleoli. In contrast, $APE1^{K4pleA}$ did not show any nucleolar accumulation. Images were captured by using the same settings (488-nm laser at 10% of intensity and PMT at 760 V). Fluorescence intensity analysis was carried out on a 25-µm-long line (white). Graphs represent the fluorescence intensity measured through a cross section of the nucleus and demonstrate an incremental fluorescence in corresponding nucleoli only in the case of $APE1^{WT}$ and $APE1^{K4pleR}$-Dendra fusion protein–expressing cells.

difference in their apparent mobility observed in SDS–PAGE was abolished when separating various mutants in urea-containing denaturing gels (Supplemental Figure S2 and unpublished data). It was also observed for other K-to-A mutants of APE1 (Fantini *et al.*, 2010). We then evaluated the contribution of the single K residues to the extent of APE1 nucleolar localization (Supplemental Figure S3) and the ability to interact with NPM1 (Figure 2B). Double mutants $APE1^{K27/35A}$, $APE1^{K31/32A}$, $APE1^{K27/35R}$, and $APE1^{K31/32R}$ and a deletion mutant lacking 33 amino acids at the protein N-terminus ($APE1^{N\Delta33}$) were compared with $APE1^{WT}$. Whereas $APE1^{WT}$, $APE1^{K27/35R}$, and $APE1^{K31/32R}$ displayed a nucleolar and nucleoplasmic staining, $APE1^{K27/35A}$ and $APE1^{K31/32A}$ showed two alternative stainings, exhibiting nucleolar/nucleoplasmic or only nucleoplasmic positivity, respectively (Supplemental Figure S3). Coimmunoprecipitation experiments (Figure 2B) were in accordance with immunofluorescence analyses and showed a substantial reduction of the interaction in the case of $APE1^{K4pleA}$ and $APE1^{N\Delta33}$ mutants and a moderate impairment for $APE1^{K27/35A}$ and $APE1^{K31/32A}$ mutants. Glutathione *S*-transferase (GST) pull-down assays with recombinant purified proteins confirmed that these results were due to effects on direct interaction between APE1 and NPM1 (Figure 2C). This confirmed previous hypotheses (Fantini *et al.*, 2010). We also checked the effect of the K-to-A mutation on the ability of APE1 to bind nucleolar rRNA (Vascotto *et al.*, 2009b). As expected, rRNA–chromatin immunoprecipitation (ChIP) analyses showed that K-to-A mutations significantly alter APE1 binding to

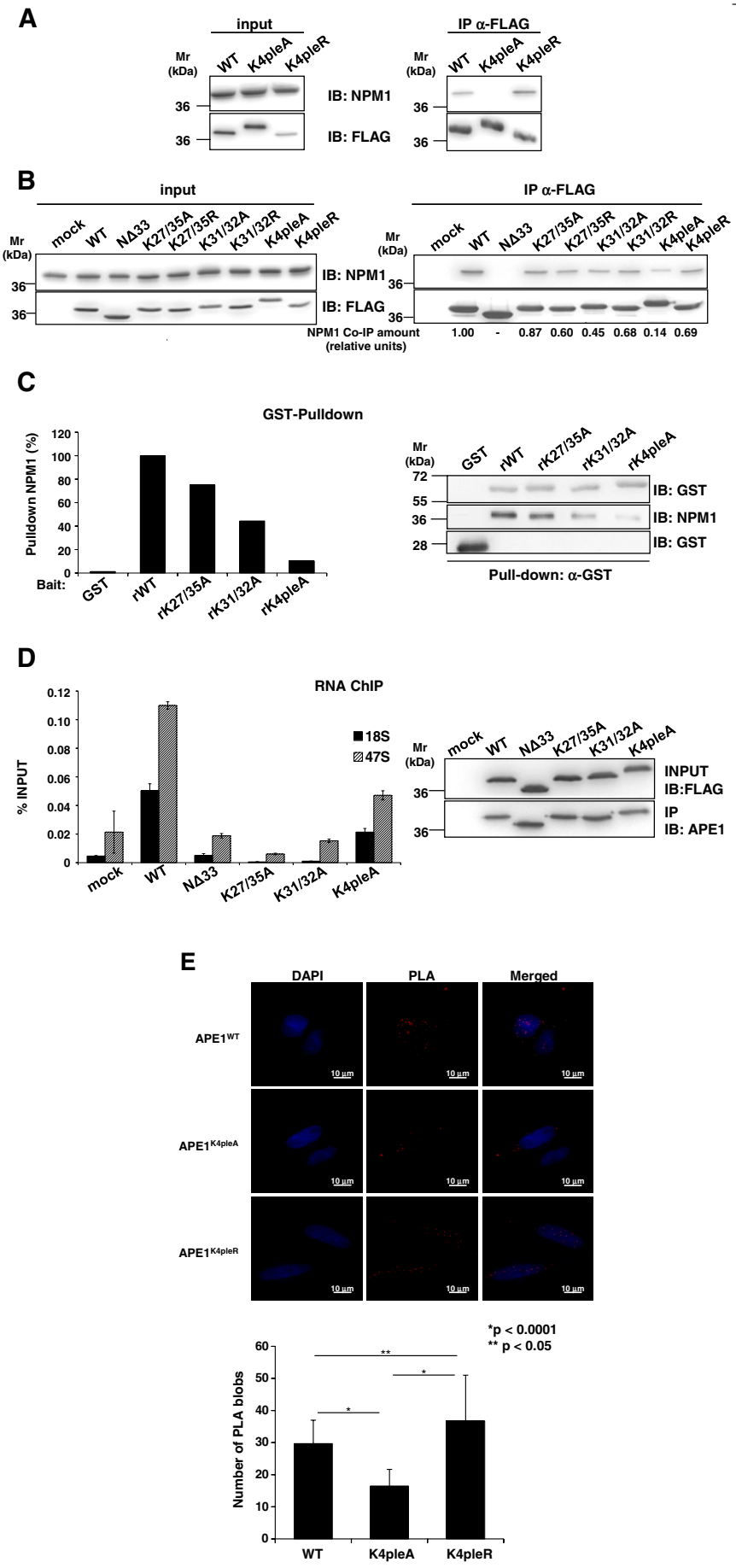

FIGURE 2: Positively charged $K^{27}/K^{31}/K^{32}/K^{35}$ residues are required for NPM1 interaction. (A) The $APE1^{K4pleA}$ mutant shows impaired interaction with NPM1. Coimmunoprecipitation (CoIP) analysis on HeLa cells transfected with $APE1^{WT}$, $APE1^{K4pleA}$, or $APE1^{K4pleR}$ FLAG-tagged proteins with endogenous NPM1. Western blot analysis was used to quantify the interaction among the different APE1 forms and NPM1 by using specific antibodies. IB, immunoblot. (B) $K^{27}/K^{31}/K^{32}/K^{35}$ residues are responsible for proper interaction of APE1 with NPM1. CoIP analysis on HeLa cells transfected with FLAG-tagged $APE1^{WT}$, $APE1^{N\Delta33}$, or the APE1 double ($APE1^{K27/35A}$, $APE1^{K31/32A}$, $APE1^{K27/35R}$, and $APE1^{K31/32R}$) or quadruple ($APE1^{K4pleA}$ and $APE1^{K4pleR}$) K-to-A or K-to-R mutants. Western blot analysis was performed on total cell extracts (left) and on immunoprecipitated material (right) with specific antibody for endogenous NPM1. Normalized coimmunoprecipitated amounts of NPM1 are indicated under each relative bar. Anti-FLAG staining was used as loading control. (C) Interaction of K-to-A APE1 mutants with NPM1 and rRNA. A 150-pmol amount of each bait GST-APE1 recombinant purified protein (rAPE1) was incubated with an equimolar amount of recombinant NPM1, as described in *Materials and Methods*. After GST pull-down, samples underwent Western blot analysis by using the indicated antibodies (right). NPM1 band intensities were normalized vs. those of GST-APE1 proteins, and the resulting values, expressed as percentage of bound with respect to $APE1^{WT}$, were plotted in the histogram (left). Each bar represents the mean of two independent experiments whose variation was <10%. (D) Interaction of K-to-A APE1 mutants with NPM1 and rRNA. After transfection of HeLa cells, total cell lysates were prepared as described in *Materials and Methods*, and an RNA-ChIP assay was performed to measure the rRNA-binding activity of the different APE1 mutants. Immunoprecipitated samples underwent either Western blot analysis (right) or RNA extraction and quantification by reverse transcription and quantitative PCR analysis, using 18S and 47S rRNA–specific primers. Data are presented as a fold percentage of the amount of total 18S or 47S rRNA with respect to the amount of immunoprecipitated FLAG-tagged APE1 protein, respectively. The resulting values are plotted in the histograms (left), showing the average values with SD of three independent experiments. (E) Nucleoplasmic interaction between APE1 and NPM1 is affected by K-to-A mutation on APE1. PLA technology was used to evaluate in vivo the effect of positively charged $K^{27}/K^{31}/K^{32}/K^{35}$ residues on APE1 interaction with NPM1 in the nuclear compartment. Stable HeLa clones expressing $APE1^{WT}$, $APE1^{K4pleA}$, or $APE1^{K4pleR}$ FLAG-tagged proteins were seeded on a glass coverslip, and PLA reaction was carried out using anti-FLAG and anti-NPM1 antibodies. 4′,6-Diamidino-2-phenylindole staining is used as a reference for the nuclei. The histogram represents the average number of PLA blobs scored for at least 30 cells per slide. Asterisks represent a significant difference between $APE1^{WT}$ and mutants.

rRNA molecules (Figure 2D) and that a partial removal of positive charges in the region 27–35 strongly affects the protein binding to rRNA molecules.

Interaction between APE1 and NPM1 may also occur in the nucleoplasmic compartment of cells. We measured the effect of the K-to-A mutation on the nucleoplasmic interaction of APE1 with NPM1 through proximity ligation assay (PLA) analysis, which allows in situ detection of two proteins that are at interacting distance of <40 nm (Weibrecht *et al.*, 2010). Data displayed in Figure 2E show that nucleoplasmic interaction between APE1 and NPM1 was significantly affected by the K-to-A mutation. Taken together, these data demonstrate that charged lysines within the 27–35 region are essential for APE1 maintenance within the nucleoli and for a proper/stable interaction of this protein with NPM1 or rRNA molecules. Moreover, our data suggest that APE1 must lose the positive charge at more than two K residues (among $K^{27}/K^{31}/K^{32}/K^{35}$) to get a significant reduction of the APE1/NPM1 interaction in the nucleus and loss of APE1 nucleolar accumulation.

Loss of APE1 nucleolar accumulation causes impairment of cell proliferation

APE1 protects cells against genotoxic damaging agents (Tell and Wilson, 2010). To clarify the biological relevance of the APE1 nucleolar accumulation, we estimated the effect of the expression of the nucleolar-deficient form of APE1 (i.e., $APE1^{K4pleA}$) on cell viability with respect to $APE1^{WT}$ and $APE1^{K4pleR}$ mutant. To test the effects of the mutant proteins and exclude the contribution of the endogenous one, we used inducible APE1-silenced (through small interfering RNA [siRNA] technology) HeLa cells, which were reconstituted with siRNA-resistant APE1 ectopic proteins in place of the endogenous one (Figure 3A; Vascotto *et al.*, 2009a). The levels of the ectopic proteins expressed by the different cell clones used for the following experiments were comparable to that of the wild-type endogenous one before silencing, as demonstrated by quantitative Western blot analysis (Supplemental Figure S4); the extent of the residual endogenous protein was <10%. Quantification of the nuclear amount of ectopic proteins after doxycycline treatment, demonstrated by Western blot analysis with a calibration curve, gave the following results (expressed as nanograms of APE1 per microgram of nuclear extract): 23.22 ± 6.04 for $APE1^{WT}$, 18.63 ± 4.84 for $APE1^{K4pleA}$, and 17.69 ±4.60 for $APE1^{K4pleR}$ (Supplemental Figure S4B). Therefore these cell lines represent a reliable system for testing our hypothesis. On the basis of previous data showing that nucleolar APE1 may act as a cleansing factor in rRNA quality control, possibly affecting cellular proliferation through an impairment of the overall protein synthesis machinery (Vascotto *et al.*, 2009b; Tell *et al.*, 2010b), we investigated the effect of the nucleolar-deficient form $APE1^{K4pleA}$ on cell proliferation rate under basal conditions. Of interest, by cell counting assays performed on reconstituted cell clones, we obtained proof that $APE1^{K4pleA}$ acts as a loss-of-function mutation in terms of cell proliferation, whereas $APE1^{K4pleR}$ behaves similarly to $APE1^{WT}$ (Figure 3B). These data, confirmed by using at least two different clones for each mutant cell line, suggest that nucleolar APE1 is required for appropriate control of cell proliferation, perhaps through its role in rRNA metabolism (Tell *et al.*, 2010b). Colony formation assays confirmed cell proliferation data (Figure 3C). However, although the cell number in each colony of $APE1^{K4pleR}$-expressing cells was always similar to that expressing $APE1^{WT}$, these cells grew in a more widespread manner, possibly due to an altered migrating phenotype and/or an intercellular adhesion pattern. These data were indicative that abolition of the acetylatable residues of APE1 at $K^{27}/K^{31}/K^{32}/K^{35}$ may significantly affect cell biology, even though it is also possible that the lower expression level of the $APE1^{K4pleR}$ (~76%) with respect to $APE1^{WT}$ may also have an effect on this phenotype.

Increased APE1 acetylation at $K^{27}/K^{31}/K^{32}/K^{35}$ residues upon genotoxic damage

APE1 acetylation at K^6/K^7 is known to be enhanced after genotoxic insult by methyl methanesulfonate (MMS) and it has been shown to play a role in modulating APE1 interaction with XRCC1, possibly coordinating different enzymatic steps in the BER pathway (Yamamori *et al.*, 2010). We therefore tested whether MMS treatment, which promotes generation of DNA damage specifically repaired through BER, may also induce APE1 acetylation at $K^{27}/K^{31}/K^{32}/K^{35}$ residues. Immunopurified APE1 samples from control and MMS-treated cells were separated by SDS–PAGE and excised bands and then analyzed by peptide mapping experiments. Semiquantitative nano–electrospray linear ion trap tandem mass spectrometry (nanoLC-ESI-LIT-MS/MS) analysis was performed on identical quantities of immunopurified $APE1^{WT}$-FLAG protein samples obtained from HeLa cells before and after MMS treatment (Supplemental Figure S5). In particular, we evaluated the amount of the peptides (15–33)Ac_3 and (15–35)Ac_4 in each APE1 endoprotease AspN digest and compared them to that of the nonmodified counterparts. Analysis was performed by extracting and integrating the corresponding nanoLC-ESI-LIT-MS peak areas equivalent to the assigned *m/z* values for the acetylated and nonacetylated peptides in the same total ion chromatogram. After MMS treatment, the amount of the peptide (15–33)Ac_3 was significantly increased, and the peptide (15–35)Ac_4 was almost doubled as compared with that of the nonmodified counterparts (Figure 4A). The MMS-induced acetylation on the aforementioned residues was further demonstrated by Western blotting using a commercial anti–Ac-Lys antibody on immunopurified proteins from HeLa cells transiently transfected with the FLAG-tagged $APE1^{WT}$ and the nonacetylatable $APE1^{K4pleR}$ forms. It is striking that a significant increase of APE1 acetylation was observed after MMS treatment but mainly for $APE1^{WT}$ rather than for $APE1^{K4pleR}$ (Supplemental Figure S6). These data show that, besides increasing the acetylation status of K^6/K^7 (see later discussion and Yamamori *et al.*, 2010), MMS treatment also promotes acetylation at $K^{27}/K^{31}/K^{32}/K^{35}$ residues. The mild increase of Lys acetylation level in the mutant $APE1^{K4pleR}$ may possibly be ascribed to K^6/K^7 acetylation (see later discussion).

We then investigated the cellular distribution pattern of acetylated APE1 at $K^{27}/K^{31}/K^{32}/K^{35}$ residues by using an ad hoc–developed antibody that specifically recognized the peptide 25–38 fully acetylated at $K^{27}/K^{31}/K^{32}/K^{35}$, hereafter referred to as anti-$APE1^{K27\text{-}35Ac}$ (Poletto *et al.*, 2012). This antibody was particularly efficient in recognizing acetylation at K^{35} with a measured affinity in the nanomolar range (196 nM for the tetra-acetylated stretch vs. 26,800 nM for the nonacetylated one, as assessed by surface plasmon resonance (SPR; Poletto *et al.*, 2012). Preincubation of the antibody with the acetylated and nonacetylated peptides confirmed the specificity of the antibody (Poletto *et al.*, 2012). The distribution pattern of $APE1^{WT}$, $APE1^{K4pleA}$, and $APE1^{K4pleR}$ was compared by using anti-FLAG and anti-$APE1^{K27\text{-}35Ac}$ antibodies. Of interest, staining with the anti-$APE1^{K27\text{-}35Ac}$ antibody gave a pattern quite similar (i.e., nucleolar exclusion) to that of the anti-FLAG antibody but only in the case of the $APE1^{K4pleA}$ mutant (Figure 4B). PLA was also carried out to demonstrate the in vivo occurrence of acetylation on endogenous APE1 by using either the anti-$APE1^{K27\text{-}35Ac}$ antibody alone (as a control) or together with an anti-APE1 antibody (Figure 4C). This assay clearly highlighted the proximity between the target of both

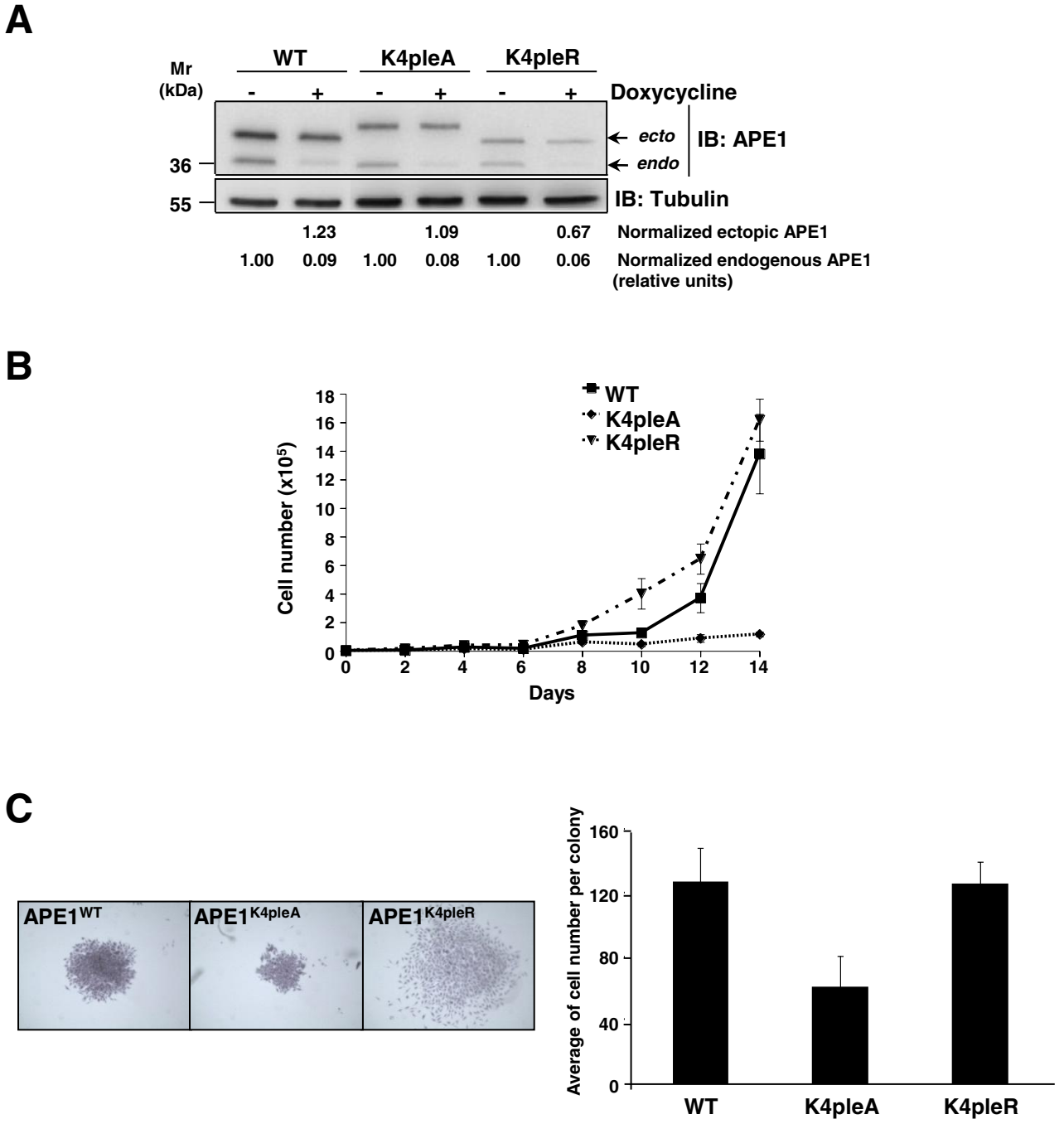

FIGURE 3: Expression of the nucleolus-deficient APE1 mutant causes impaired cell proliferation. (A) Generation of reconstituted cell lines expressing APE1^{K4pleA} and APE1^{K4pleR} mutants. HeLa cells were stably transfected with the inducible siRNA vectors and siRNA resistant APE1^{WT}, APE1^{K4pleA}, and APE1^{K4pleR}–expressing vectors, as previously described (Vascotto *et al.*, 2009a; Fantini *et al.*, 2010). Expression of ectopic APE1 forms without silencing and after the suppression of endogenous APE1 expression after 10 d of treatment with doxycycline (Doxy) was assayed by Western blotting on total cellular extracts with an anti-APE1 antibody. Normalized expression levels for each clone of ectopic and endogenous APE1 protein after the silencing are indicated under each relative band. β-Tubulin was used as loading control. (B) Cell proliferation assays for APE1-reconstituted cell lines. APE1-expressing cell clones were seeded in 60-mm Petri dishes. Growth was followed by measuring cell numbers at various times upon doxycycline treatment, as indicated. Cells were harvested at the indicated times, stained with trypan blue, and counted in triplicate. Data, expressed as cell number, are the mean ± SD of three independent experiments. (C) Colony formation assays for APE1-reconstituted cell lines. After 8 d of doxycycline treatment, 200 cells of APE1^{WT} and the indicated APE1 mutants were seeded in 60-mm Petri dishes and grown for 8 d in medium supplemented with doxycycline to promote endogenous APE1 silencing. Then cells were stained with crystal violet and images captured by using a Leica S8 microscope with 80× magnification. Data, expressed as number of cells per colony, are the mean ± SD of 10 colonies for each clone.

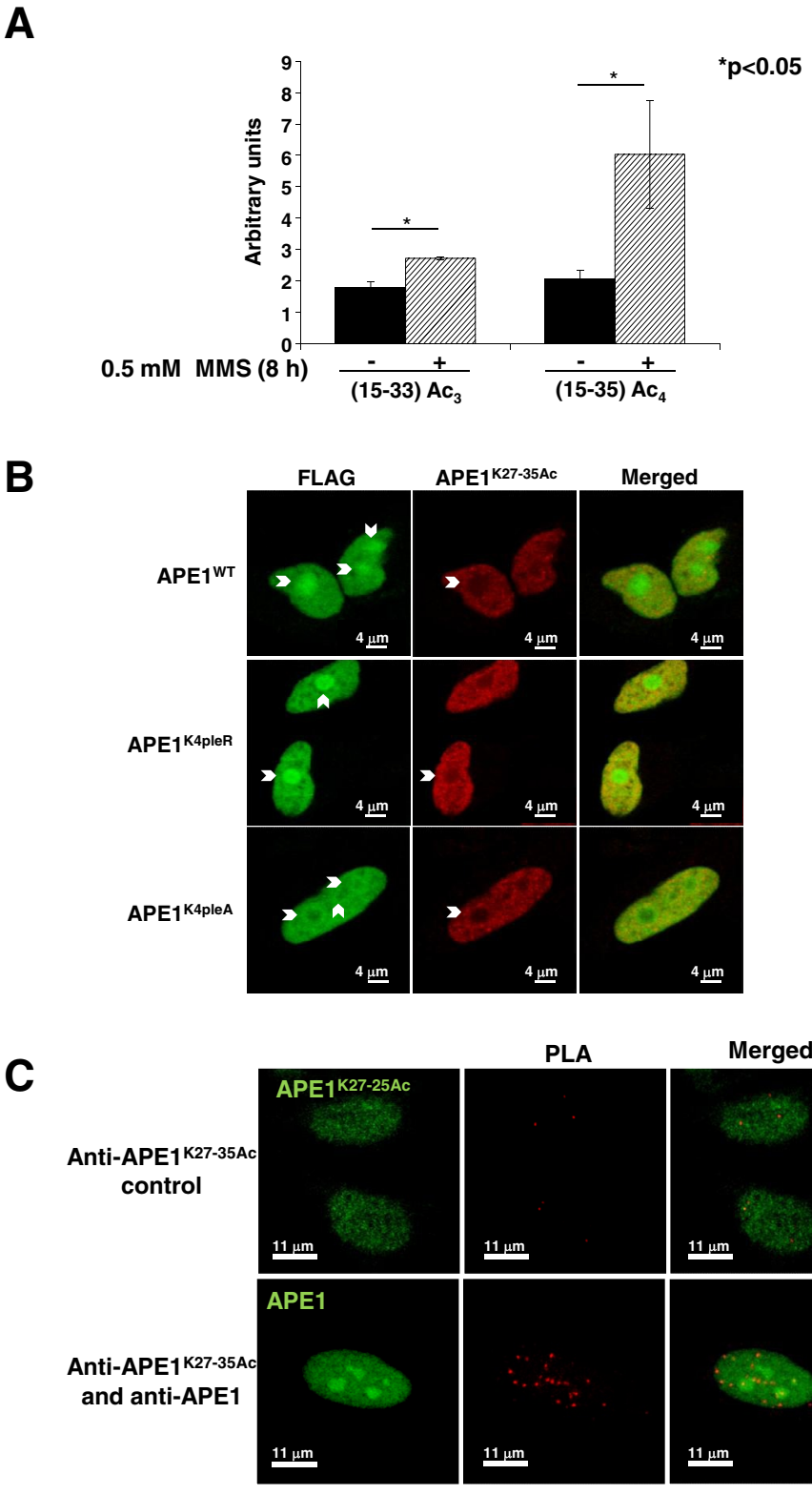

FIGURE 4: Genotoxic treatment promotes APE1 acetylation at $K^{27}/K^{31}/K^{32}/K^{35}$ residues. (A) Relative quantitative changes of APE1 acetylation at $K^{27}/K^{31}/K^{32}/K^{35}$ after MMS treatment. Mass spectrometry analysis of acetylated peptides present in the endoprotease AspN digest of FLAG-tagged $APE1^{WT}$ purified from HeLa cells (see *Materials and Methods* for details). Histograms indicate the relative amounts of the peptides (15–33)Ac_3 and (15–35)Ac_4 with respect to their nonmodified counterparts before and after MMS treatment. Identical ionization tendencies were assumed for each peptide pair. Each bar represents the mean of three independent experiments. (B) Acetylated APE1 at $K^{27}/K^{31}/K^{32}/K^{35}$ residues is present within cell nucleoplasm but is excluded from nucleoli. Confocal microscopy of HeLa cells transfected with $APE1^{WT}$, $APE1^{K4pleA}$, or $APE1^{K4pleR}$ FLAG-tagged proteins and stained with antibodies against endogenous $APE1^{K27–35Ac}$ (anti-$APE1^{K27–35Ac}$, red) and ectopic APE1 FLAG-tagged (green). Overlap of staining (yellow) demonstrated the codetection of the two protein forms. Images are representative of 100% of transfected cells. (C) APE1 acetylation at $K^{27}/K^{31}/K^{32}/K^{35}$ occurs in vivo. PLA signal obtained using the anti-$APE1^{K27–35Ac}$ antibody together with the anti-APE1 antibody on fixed HeLa cells. A technical control, using the anti-$APE1^{K27–35Ac}$ antibody alone, was introduced (top). Nuclei were counterstained using an Alexa Fluor 488–conjugated secondary anti-rabbit (recognizing the endogenous $APE1^{K27–35Ac}$, in the control reaction) or anti-mouse antibody (recognizing the endogenous APE1 protein in the PLA reaction; green).

antibodies, further suggesting that, in vivo, APE1 is acetylated at $K^{27}/K^{31}/K^{32}/K^{35}$ residues and that these acetylated forms are excluded from the nucleoli. Taken together, these data suggest that acetylation at these charged amino acids may control the nucleolar/nucleoplasmic distribution of APE1 within cells.

Removal of positively charged $K^{27}/K^{31}/K^{32}/K^{35}$ residues increases APE1 DNA-repair activity in vivo

We tested whether abolition of positive charges on acetylatable residues may affect the APE1 DNA repair function in cells, as previously demonstrated in vitro by using recombinant purified proteins bearing two different clusters of K-to-A mutation (i.e., on residues 24/25/27 and on residues 24/25/27/31/32; Fantini *et al.*, 2010). For this purpose we used nuclear extracts from reconstituted cell clones after precise normalization for the APE1 ectopic nuclear content with a titration curve (as shown in Supplemental Figure S4). This normalization for APE1 ectopic protein expression allowed comparison of the enzymatic activities of the different protein mutants in the nuclear fractions from each clone. Figure 5A shows that the AP-endonuclease activity of the $APE1^{K4pleA}$ mutant, measured through cleavage assays performed with nuclear extracts, was significantly increased with respect to $APE1^{WT}$-and $APE1^{K4pleR}$-expressing cells. Moreover, Figure 5B shows a lower amount of abasic DNA lesions accumulated after MMS treatment by the $APE1^{K4pleA}$- as compared with the $APE1^{WT}$-expressing cells. These results suggest that removal of positive charges at Lys 27–35, as exerted by acetylation, may result in a more enzymatically active protein.

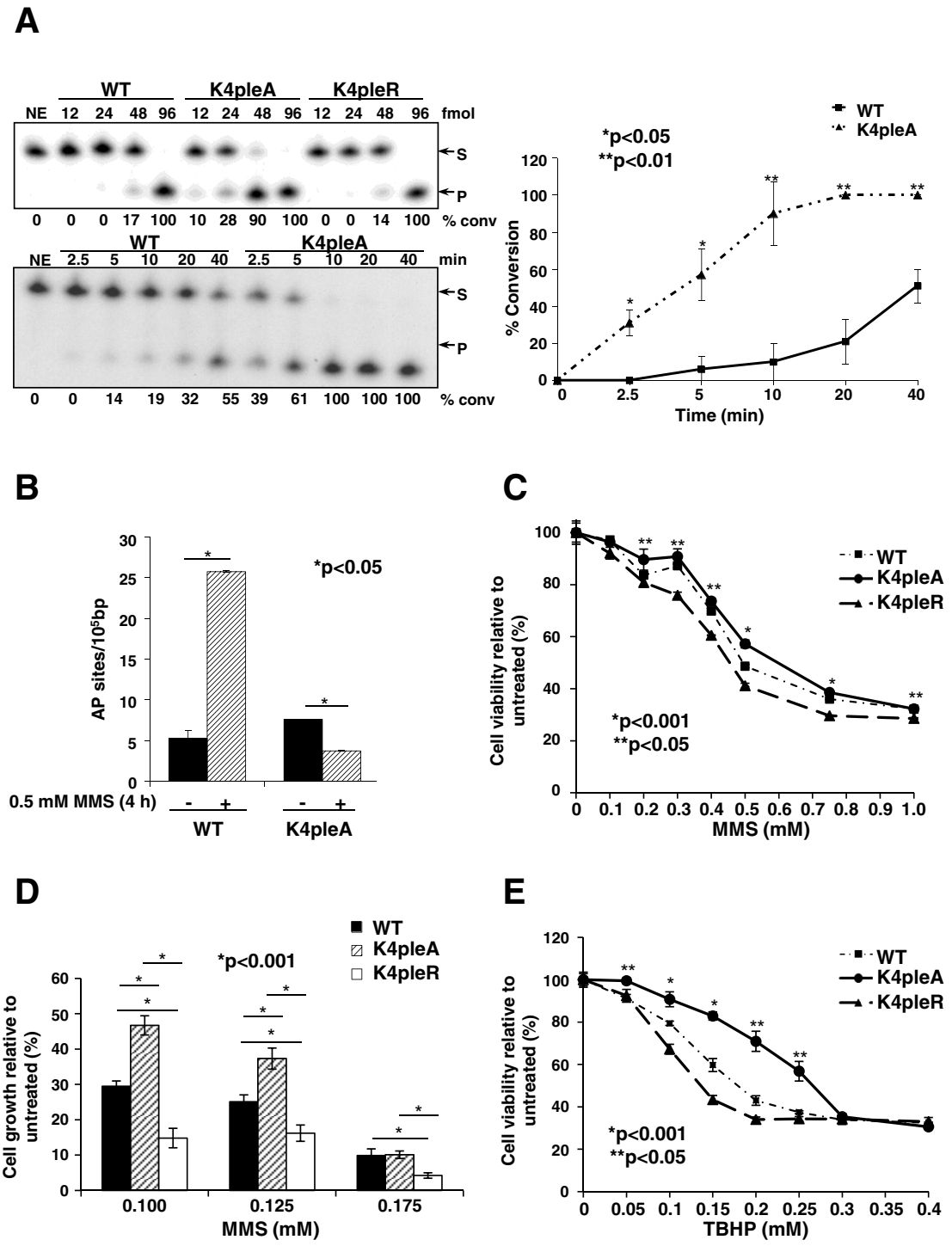

FIGURE 5: Abolition of positively charges $K^{27}/K^{31}/K^{32}/K^{35}$ residues increases APE1 DNA-repair activity. (A) Nuclear extracts from $APE1^{K4pleA}$ mutant present an increased AP endonuclease activity on abasic DNA. AP-site incision activity of the nuclear extracts from HeLa-reconstituted cell clones was tested using an AP endonuclease activity assay as described in *Material and Methods*. The nuclear APE1 content in each clone was precisely quantified through a titration curve obtained using purified recombinant APE1 (Supplemental Figure S4). Nuclear ectopic APE1 protein levels were then normalized between the different cell clones in order to compare their relative enzymatic activities. Top left, concentration-dependent conversion of an AP site–containing DNA substrate (S) to the incised product (P). A representative image of the denaturing polyacrylamide gel of the enzymatic reactions is shown. The amounts (femtomoles) of APE1 used in the reaction and the percentage of substrate converted into product, as determined by standard phosphorimager analysis, are indicated. NE, no cell extract control. Bottom left, time-dependent kinetics of APE1 (2.15 ng) endonuclease activity from nuclear extracts of the different reconstituted cell clones. The image of a representative gel analysis is shown (bottom). Right, graph depicting the time-course kinetics of APE1 from incision results shown on the left. Average values are plotted ± SD of three independent experiments. Asterisks represent a

Cell viability experiments, after MMS treatment, were carried out to verify the enzymatic data. Thus, the effect of $K^{27}/K^{31}/K^{32}/K^{35}$ mutation on cell viability after MMS treatment was measured by 3-(4-5-dimethylthiazol-2-yl)-5-(3-carboxymethoxyphenyl)-2-(4-sulfophenyl)-2H-tetrazolium salt (MTS) and clonogenic assays using the reconstituted cell clones. The MTS data (Figure 5C) showed that the $APE1^{K4pleA}$-mutant–expressing cells were significantly more resistant to MMS treatment than those expressing the nonacetylatable $APE1^{K4pleR}$ mutant. Of note, clonogenic assay experiments (Figure 5D) confirmed these results and highlighted the relevant acetylation occurring at the K residues, as demonstrated by the higher sensitivity of $APE1^{K4pleR}$-expressing cells after MMS treatment. We extended our observations on the protective function of the $APE1^{K4pleA}$ mutant by using *tert*-butyl-hydroperoxide (TBHP) as a reactive oxygen species (ROS) generator (Lazzé *et al.*, 2003). We recently demonstrated that APE1 knockdown sensitizes HeLa cells to TBHP treatment (Li *et al.*, 2012). Therefore we now measured the sensitivity of the different reconstituted cell clones to TBHP in a dose–response experiment (Figure 5E). As in the case of MMS treatment, expression of the $APE1^{K4pleA}$ mutant exerted a protective function with regard to TBHP treatment with respect to $APE1^{WT}$-expressing cells. Similarly to MMS treatment, the $APE1^{K4pleR}$-mutant–expressing clone evidenced even more sensitivity than the $APE1^{WT}$-expressing one. Taken together, these data show that acetylation at residues $K^{27}/K^{31}/K^{32}/K^{35}$ is associated with cell response to DNA damage and confers protection to genotoxic treatment. The increased activity of the $APE1^{K4pleA}$ mutant may explain its proficient protective effect in vivo against genotoxic treatment, even though further explanatory mechanisms, such as its altered protein association in the cell or its possible higher stability (Vascotto *et al.*, 2011), could also be invoked.

K^6/K^7 deacetylation by SIRT1 is modulated by the charged status of $K^{27}/K^{31}/K^{32}/K^{35}$residues

It was recently demonstrated that APE1 K^6/K^7 may undergo acetylation during cell response to genotoxic treatment (Fantini *et al.*, 2008; Yamamori *et al.*, 2010) and that modulation of the acetylation status of these residues through SIRT1 deacetylase activity is important for the regulation of APE1 DNA-repair function after MMS treatment (Yamamori *et al.*, 2010). However, the molecular mechanism regulating the SIRT1-mediated modification at these amino acids during MMS treatment is unknown. We thus checked whether the charged status of $K^{27}/K^{31}/K^{32}/K^{35}$ residues might play a role in modulating the acetylation status of K^6/K^7 through the contribution of SIRT1. First, we evaluated the effect of the modification at $K^{27}/K^{31}/K^{32}/K^{35}$ on the ability of SIRT1 to deacetylate K^6/K^7 in APE1. We found that recombinant purified APE1 protein is nonenzymatically acetylated after incubation with acetyl-CoA, as demonstrated for other proteins (Garbutt and Abraham, 1981). Thus, to obtain a significant amount of acetylated recombinant APE1 protein on K^6/K^7 residues, we treated purified recombinant rAPE1 obtained from *E. coli* with acetyl-CoA, as described in the Supplemental Information. Then we treated in vitro–acetylated $rAPE1^{WT}$, $rAPE1^{K4pleA}$, $rAPE1^{K27/35A,}$ or $rAPE1^{K31/32A}$ with purified recombinant SIRT1 protein and measured the acetylation level on K^6/K^7 through a specific antibody that recognizes only acetylation at these residues (Fantini *et al.*, 2008; Sengupta *et al.*, 2011). Of interest, although $APE1^{WT}$ was efficiently deacetylated by SIRT1 at K^6/K^7 (Figure 6A), the $APE1^{K4pleA}$ mutant did not show any deacetylation in this region; concomitant K-to-A substitutions at positions 27 and 35 ($APE1^{K27/35A}$ mutant) or at positions 31 and 32 ($APE1^{K31/32A}$ mutant) caused an intermediate effect.

We then verified the ability of SIRT1 to directly deacetylate APE1 at $K^{27}/K^{31}/K^{32}/K^{35}$ residues through in vitro deacetylation assays carried out on acetylated purified recombinant $rAPE1^{WT}$ or mutant proteins as substrates (Supplemental Figure S7). Protein acetylation level was monitored by using the anti-$APE1^{K27\text{-}35Ac}$ (Figure 6B). Incubation with recombinant-purified SIRT1 protein revealed a marked decrease in acetyl-APE1 signal but only when $APE1^{WT}$ was used. These data were corroborated by qualitative peptide mapping experiments on in vitro–acetylated $rAPE1^{WT}$ before and after incubation with SIRT1. This analysis demonstrated that SIRT1 was indeed able to deacetylate in vitro–acetylated $rAPE1^{WT}$ at least at $K^{25}/K^{27}/K^{32}$ residues (Supplemental Table S1).

The ability of SIRT1 to deacetylate in vitro APE1 at $K^{27}/K^{31}/K^{32}/K^{35}$ was also analyzed on APE1 (25–38) peptides (Figure 6C), which were chemically synthesized either in their nonacetylated or tetra-acetylated form at these K residues. These peptides were used in a competitive fluorescence-based assay in which a fluorogenic p53 acetylated peptide was used as SIRT1 substrate (Marcotte *et al.*, 2004). As expected, we observed a dose-dependent decrease in the

significant difference between $APE1^{WT}$ and $APE1^{K4pleA}$. (B) Accumulation of genomic abasic (AP) lesions after MMS treatment (0.5 mM, 4 h) of reconstituted cell clones with $APE1^{WT}$ and $APE1^{K4pleA}$ mutant as measured by an aldehyde-reactive probe. $APE1^{WT}$ and $APE1^{K4pleA}$-expressing HeLa cells were grown in medium supplemented with Doxy (10 d) to silence endogenous APE1 expression and were treated with 0.5 mM MMS for 4 h. Counting at the AP sites was performed by using the AP-site quantification kit, as described in *Materials and Methods*. In the histogram, data are expressed as number of AP sites per 10^5 base pairs and represent the mean ± SD of four independent experiments. Asterisks represent a significant difference between the two conditions (untreated and MMS-treated cells). (C) Effects of APE1 acetylation mutants on cell viability after MMS treatment in reconstituted cells. $APE1^{WT}$, $APE1^{K4pleA}$-, and $APE1^{K4pleR}$-expressing cells were grown in medium supplemented with Doxy to silence APE1 endogenous protein and treated with increasing concentrations of MMS for 8 h; the cytotoxic effect of this compound was determined by the MTS assay (see *Materials and Methods* for details). Each point, shown as percentage viability with respect to untreated clones, represents the mean ± SD of four observations, repeated in at least two independent assays. Asterisks represent a significant difference between $APE1^{K4pleA}$ and $APE1^{K4pleR}$ mutants. (D) Cell growth as measured by colony survival assay. One thousand cells of $APE1^{WT}$-, $APE1^{K4pleA}$-, and $APE1^{K4pleR}$-expressing clones treated with increasing concentrations of MMS for 8 h were seeded in Petri dishes and then treated with Doxy for 10 d to silence endogenous APE1. Data, expressed as the percentage of change with respect to untreated clones, are the mean ± SD of three independent experiments. (E) Effects of APE1 acetylation mutants on cell viability after TBHP treatment in $APE1^{WT}$-, $APE1^{K4pleA}$-, and $APE1^{K4pleR}$-expressing cells grown in medium supplemented with Doxy to silence APE1 endogenous protein. Cells were treated with increasing concentrations of TBHP for 6 h, and the cytotoxic effects were determined by the MTS assay. Each point, shown as percentage viability with respect to untreated clones, represents the mean ± SD of four observations, repeated in at least two independent assays. Asterisks represent a significant difference between $APE1^{K4pleA}$ and $APE1^{K4pleR}$ mutants.

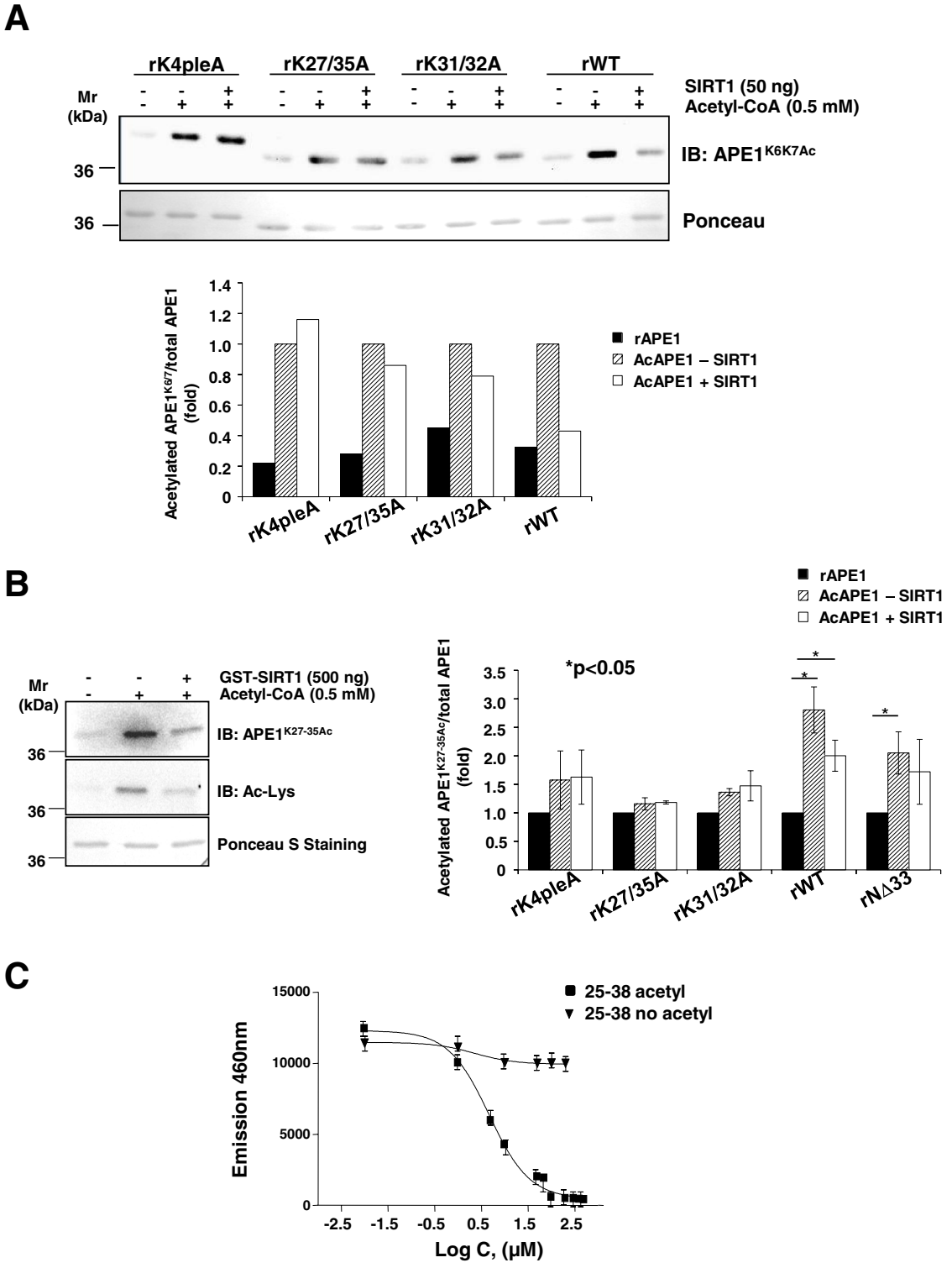

FIGURE 6: SIRT1 deacetylase activity on K^6/K^7 depends on the charged status of $K^{27}/K^{31}/K^{32}/K^{35}$ residues. (A) K^6/K^7 acetylation, modulated by SIRT1, depends on the charged status of $K^{27}/K^{31}/K^{32}/K^{35}$ residues. Western blot analysis on purified recombinant APE1 proteins in vitro acetylated with acetyl-CoA and then incubated in the presence/absence of recombinant GST-SIRT1, as indicated. The analysis was carried out using an antibody specific for acetylated K^6/K^7 APE1 (top). The histogram reports data obtained from densitometric quantification of the bands for each APE1 protein after normalization on Ponceau S staining (bottom). Data shown are the mean of two independent experimental sets whose variation was <10%. (B) SIRT1 deacetylates rAPE1 at $K^{27}/K^{31}/K^{32}/K^{35}$. Left, Western blot analysis on the in vitro–acetylated and deacetylated purified recombinant APE1, further subjected to MS analysis (Supplemental Table S1). $rAPE1^{WT}$ was incubated with 0.5 mM acetyl-CoA and then with recombinant SIRT1 protein, as shown. Samples were separated onto 10% SDS–PAGE, and Western blot analysis was performed by using the anti-$APE1^{K27-35Ac}$ antibody. Ponceau S staining was used as loading control. Right, the histogram shows the densitometric quantification of the

fluorescence signal by using different amounts of the tetra-acetylated peptide (25–38); the nonacetylated counterpart was used as a negative control substrate. Best data fitting was observed with a one-site competition equation, which provided an IC_{50} value of 4.6 ± 0.3 μM. These data support the conclusion that the acetylated APE1 region spanning amino acids 27–35 is a substrate for SIRT1 deacetylase activity. Taken together, these results demonstrate that SIRT1's ability to efficiently deacetylate APE1 at K^6/K^7 residues relies on the presence of positive charges at $K^{27}/K^{31}/K^{32}/K^{35}$. Moreover, SIRT1 is also able to bind and possibly deacetylate in vitro–acetylated APE1 $K^{27}/K^{31}/K^{32}/K^{35}$ residues.

Cross-talk between the charged state of $K^{27}/K^{31}/K^{32}/K^{35}$ and the acetylation status of K^6/K^7 residues through SIRT1

To understand whether SIRT1 activity on acetylated K^6/K^7 residues might be modulated in vivo by MMS as a function of the charged status of $K^{27}/K^{31}/K^{32}/K^{35}$, we performed coimmunoprecipitation experiments on transiently transfected HeLa cells. As shown in Figure 7A, an intact N-terminal domain is required for stable APE1 binding to SIRT1. The APE1/SIRT1 association was induced after MMS treatment and was abolished in the case of both $APE1^{N\Delta33}$ and $APE1^{K4pleA}$ mutants. Substitution of $K^{27}/K^{31}/K^{32}/K^{35}$ residues with nonacetylatable R residues was ineffective, suggesting that SIRT1 binding depends on the presence of positively charged amino acids spanning the APE1 region 27–35. Measurements of K^6/K^7 acetylation status with the specific antibody (performed on the same samples) clearly showed that, in agreement with the binding data, K^6/K^7 residues resulted in more acetylation both under basal and after MMS treatment but only in the case of the $APE1^{K4pleA}$ mutant. In addition, the acetylation status of $APE1^{WT}$ and $APE1^{K4pleR}$, both under basal conditions and after MMS treatment, was comparable (Figure 7B), supporting the existence of cross-talk between the charged status of $K^{27}/K^{31}/K^{32}/K^{35}$ and the acetylation level of K^6/K^7.

We then investigated the cross-talk between K^6/K^7 and $K^{27}/K^{31}/K^{32}/K^{35}$ acetylation status through siRNA experiments. HeLa cell lines stably expressing both endogenous APE1 and $APE1^{WT}$, $APE1^{K4pleA}$, and $APE1^{K4pleR}$ ectopic forms were silenced for SIRT1 expression as described in *Materials and Methods*. The acetylation level of K^6/K^7 was then measured through Western blotting. Data shown in Figure 7C demonstrate that the K^6/K^7 acetylation level of the ectopic APE1 forms was increased ~30–40% upon SIRT1 silencing but only in the case of $APE1^{WT}$- and $APE1^{K4pleR}$-expressing cells, whereas acetylation of K^6/K^7 of $APE1^{K4pleA}$ was <10%. As a control, the acetylation level of endogenous APE1 always increased (~60–70%) upon SIRT1 silencing in all the cell lines tested (unpublished data). Taken together, these data demonstrate that the acetylation/charged status of $K^{27}/K^{31}/K^{32}/K^{35}$ residues controls the stability of the SIRT1/APE1 complex, thus playing a role in the acetylation level of K^6/K^7.

Possible relevance of acetylation for APE1 subnuclear distribution and protein local conformation

The data suggest that a coordinated acetylation/deacetylation dynamic modulated by SIRT1 may occur within the cell nucleus and could be responsible for APE1 subnuclear trafficking. Thus, we examined the subnuclear distribution of SIRT1 on c-myc-SIRT1–transfected cells through immunofluorescence analysis. We found that transiently transfected c-myc-SIRT1 mainly localized in the nucleoplasmic compartment and was not found in the nucleoli (Figure 8A, left); quantification of the endogenous SIRT1 protein in biochemically purified nucleoli confirmed its absence from this subnuclear compartment (Figure 8A, right). Evaluation of the acetylation status of APE1 present in nucleolar or nucleoplasmic fractions under basal conditions showed that APE1 acetylated at K^6/K^7 is mainly present within the nucleoplasm but almost absent in the nucleolus (Figure 8B). Of note, these findings may have important implications for SIRT1-mediated deacetylation at K^6/K^7 and demonstrate the possibility that APE1 acetylation modulates the protein's subnuclear distribution and enzymatic functions, corroborating our previous work (Fantini *et al.*, 2010).

It is known that Lys acetylation may control local conformational stability of proteins, thus affecting their activity, subcellular distribution, and protein–protein interaction network. To examine the effect of acetylation on the local structure of the N-terminal APE1 region, we analyzed the conformational behavior of the protein portion of residues 14–38, which contain $K^{27}/K^{31}/K^{32}/K^{35}$ residues acetylatable in vivo. To this end, we chemically synthesized and purified four peptides bearing differential acetylation at positions 27, 31, 32, and 35 (Supplemental Table S2). To evaluate the effect of acetylation on peptide conformation, we undertook structural analysis of these peptides in solution by far-ultraviolet (UV) circular dichroism (CD) and nuclear magnetic resonance (NMR) spectroscopy. Figure 8C shows the overlay of CD spectra of APE1(14–38) and $APE1(14–38)^{K27/31/32/35Ac}$ in aqueous buffer, indicating a minimum at ~200 nm and a shoulder at ~220 nm. These features suggest the presence of mixed conformational states in which an unfolded state coexists with a certain helical content. The propensity of this domain to adopt helical conformation was also confirmed by trifluoroethanol (TFE) titration experiments (Supplemental Figure S8A). In particular, the CD spectrum of the tetra-acetylated peptide showed a minimum at 220 nm that was deeper than that of the nonacetylated counterpart, suggesting a role for the acetyl groups in determining structural changes in this protein region. An intermediate behavior was observed for the monoacetylated and triacetylated peptides, confirming the role of this K modification in modulating the conformation of the N-terminal APE1 region (unpublished data).

To further address this point, we carried out additional NMR experiments. In aqueous buffer, the one-dimensional (1D) spectra presented poor signal dispersion (Figure 8D, left), confirming a rather disordered state for both the tetra-acetylated and nonacetylated peptides. This observation was further strengthened by the analysis of two-dimensional (2D) [^{1}H, ^{1}H] total correlation spectroscopy (TOCSY) spectra (Griesinger *et al.*, 1988; Figure 8D, middle), and 2D [^{1}H, ^{1}H] rotating frame nuclear Overhauser effect spectroscopy (ROESY) spectra (Bax and Davis, 1985; Figure 8D, right). In the latter case, the presence of a restricted set of cross-peaks in the $_N$H-aliphatic side-chain proton correlation region made unfeasible the process of sequential resonance assignments, as often occurs for small, flexible

band intensities, after normalization to the nonacetylated APE1 form, of the in vitro–acetylated and deacetylated purified APE1 mutants. Data are the mean ± SD of three independent replicates. Asterisks represent a significant difference. (C) The acetylated APE1 25–38 peptide is a substrate of SIRT1 activity. Purified APE1 peptides (25–38) either in fully acetylated form at $K^{27}/K^{31}/K^{32}/K^{35}$ residues or not acetylated were analyzed as competitors in an in vitro deacetylase SIRT1 assay based on a fluorogenic acetylated peptide derived from p53 (region 379–382). Dose–response signals allowed an estimated IC_{50} value of 4.6 ± 0.3 μM of the acetylated APE1 25–38 region with respect to the p53 peptide.

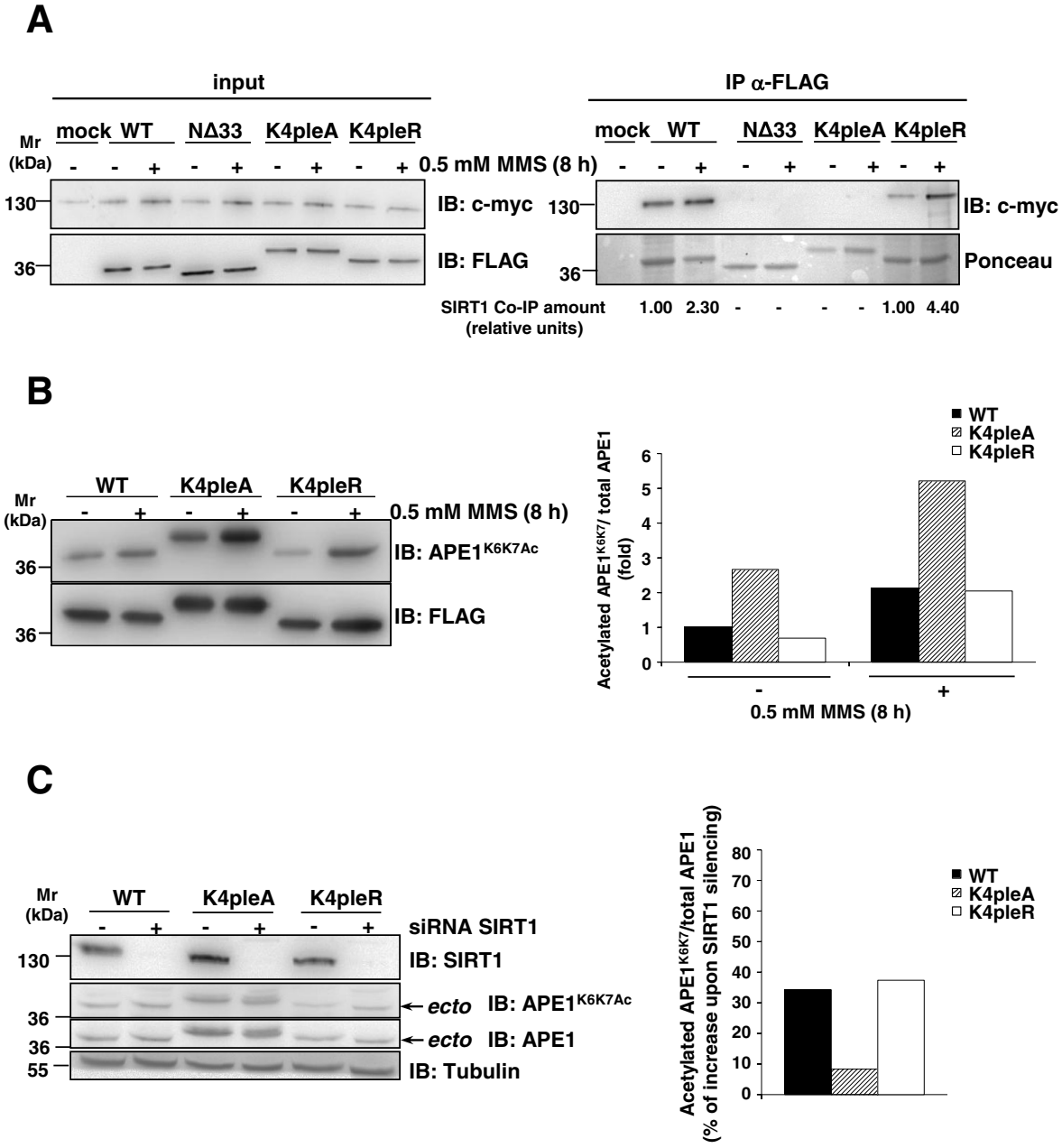

FIGURE 7: Cross-talk between the acetylation status of $K^{27}/K^{31}/K^{32}/K^{35}$ and K^6/K^7 residues through SIRT1. (A) Positive charges at $K^{27}/K^{31}/K^{32}/K^{35}$ residues strongly influence the stability of SIRT1 binding to APE1. Western blot analysis performed on total cell extracts (left) and on immunoprecipitated material (right) from HeLa cells cotransfected with c-myc–tagged SIRT1 and $APE1^{WT}$, $APE1^{N\Delta33}$, $APE1^{K4pleA}$, or $APE1^{K4pleR}$ FLAG-tagged proteins and treated with 0.5 mM MMS for 8 h. Coimmunoprecipitated amounts of SIRT1 normalized with respect to $APE1^{WT}$ or $APE1^{K4pleR}$, respectively, are indicated under each relative bar. Ponceau S staining was used as loading control. (B) Acetylation level of K^6/K^7 in $APE1^{K4pleA}$ mutant is higher than that of $APE1^{WT}$ both under basal conditions and after MMS treatment. Western blot analysis on CoIP material after MMS treatment from HeLa cells transfected with $APE1^{WT}$ and FLAG-tagged mutants is shown. The histogram indicates the relative amount of acetylated $APE1^{K6/K7}$ in the different clones obtained from the densitometric quantification of acetylated APE1 bands, normalized with respect to the amount of APE1 FLAG-tagged immunopurified protein. Data shown are the mean of two independent experimental sets whose variation was <10%. (C) SIRT1 siRNA knockdown increases APE1 K^6/K^7 acetylation. HeLa stable clones expressing $APE1^{WT}$, $APE1^{K4pleA}$, and $APE1^{K4pleR}$ were transfected with siRNA against SIRT1 protein or control siRNA. Western blot analysis was performed to detect differential amount of the acetylated K^6/K^7 APE1 after SIRT1 silencing. Arrows highlight bands of ectopic APE1 protein form; β-tubulin was used as a loading control. The histogram shows densitometric quantification of acetylated K^6/K^7 APE1 form. Data are expressed as percentage of induction of the acetylated K^6/K^7 APE1 after SIRT1 silencing after normalization for the total APE1 protein levels. Data shown are the mean of two independent experimental sets whose variation was <10%.

peptides that tumble very rapidly in solution. On the other hand, a detailed comparison of the 1D NMR data for the nonacetylated and tetra-acetylated APE1 peptides (Figure 8D, left) indicated that acetylation causes a small but clear improvement of spectral dispersion, which can be particularly appreciated in the $_N$H region (Figure 8D, top left). Moreover, the intensity of ROE cross-peaks is increased in the spectra of APE1(14-38)$^{K27/31/32/35Ac}$ peptide as compared with the nonmodified counterpart (Figure 8D, right). This evidence, together with small chemical shift changes, point toward the presence of more organized conformations for the tetra-acetylated peptide in aqueous solution, in agreement with CD data. Similar conclusions are drawn from the analysis of NMR data for APE1(14–38) and APE1(14–38)$^{K27/31/32/35Ac}$ peptides in phosphate:TFE solution (Supplemental Figure S8B), which suggested again the higher propensity of this domain in its acetylated form to adopt a more ordered conformation in contrast to the nonmodified counterpart. Also in this case, monoacetylated and triacetylated peptides showed an intermediate behavior (unpublished data). These data suggest that acetylation may account for local conformational changes on APE1 structure that may modulate its binding ability to different substrates.

DISCUSSION

APE1 is an unusually abundant DNA-repair protein in mammalian cells, with a wide nuclear distribution and an essential role in the BER pathway of DNA lesions (Tell and Wilson, 2010). We calculated that HeLa cells express ~4 × 10^7 molecules per cell (Supplemental Figure S4A), whereas other enzymes of the BER pathway, such as Pol β or XRCC1, are present at an extent of <1/10 (Demple and DeMott, 2002; Parsons *et al.*, 2008). Therefore APE1 involvement in preformed DNA-repair complexes may only partially explain the energy cost used to maintain such high protein concentration within the cells. Recently we found that APE1 may interact with rRNA and with proteins involved in RNA metabolism and is associated with nucleolar structures through its interaction with NPM1 (Vascotto *et al.*, 2009b; Tell *et al.*, 2010b). Interaction with rRNA and NPM1 strictly depends on the positive charge of K residues within the APE1 region 24–35 placed within the unstructured protein N-terminal domain, as demonstrated by the inability of the corresponding K-to-A mutants (resembling constitutive acetylation at these residues) to stably bind both rRNA and NPM1 (Fantini *et al.*, 2010). Of interest, some of these amino acids (i.e., $K^{27}/K^{31}/K^{32}/K^{35}$), which have been acquired during evolution, may undergo in vivo acetylation (Fantini *et al.*, 2010). We conjectured that, under physiological conditions, nonacetylated APE1 may be stored in the nucleolar compartment through its binding to NPM1 and rRNA, but the in vivo relevance of APE1 nucleolar accumulation was still unclear. This study was aimed at addressing this issue.

We also found that APE1^{K4pleA} binds poorly to NPM1 and rRNA in vivo and as a result is unable to accumulate within the nucleoli, whereas it is present in the nucleoplasm. Moreover, reconstitution of HeLa cells with this mutant gave improved protection from genotoxic damage induced by alkylating agents, such as MMS, and oxidative stress-generating compounds, such as TBHP, through increased DNA-repair activity. As expected for a regulated phenomenon such as the response to a genome insult, an in vivo–augmented acetylation at $K^{27}/K^{31}/K^{32}/K^{35}$ residues was observed during cell response to genotoxic damage. Furthermore, cross-talk involving the SIRT1 deacetylase occurred within cells between acetylation at $K^{27}/K^{31}/K^{32}/K^{35}$ and at K^6/K^7 residues. Therefore we hypothesized that genotoxic stress may shift the equilibrium between the nonacetylated and acetylated APE1 forms toward the latter, which would result in the most enzymatically active one on abasic DNA. This also corresponds to our previous data obtained in vitro with recombinant purified proteins (Fantini *et al.*, 2010). In many cases, the presence of the unstructured N-terminal domain of APE1 seemed essential for interaction of APE1 with different substrates (i.e., nucleic acids or proteins). Interaction also increased after histone deacetylase (HDAC) inhibition, which promotes APE1 acetylation at K^6/K^7 residues (Bhakat *et al.*, 2003; Yamamori *et al.*, 2010). This evidence strongly support the notion that this unstructured domain is responsible for the modulation of APE1's different functions through the recruitment of APE1 in different protein complexes by means of various amino acid side-chain modification events. From an evolutionary perspective, it can be hypothesized that mammalian APE1 activity was made adjustable (through PTMs and/or interaction with other proteins), or expanded toward other substrates, with the acquisition of a protein N-terminus containing positively charged residues, without major modifications on the enzyme catalytic site, which retained the "canonical" function toward abasic DNA. The existence of such an N-terminal extension in only mammals may suggest its evolutionary significance in the face of increased functional complexity. For the noncomplexed protein in solution, the intrinsic lack of a secondary structure associated with this domain can confer functional advantages to mammalian APE1, including the ability to bind to different protein targets (e.g., NPM1, XRCC1, CSB, RNA, etc.; Vidal *et al.*, 2001; Wong *et al.*, 2007; Vascotto *et al.*, 2009a; Tell *et al.*, 2010a), thus allowing efficient control over the thermodynamics in the binding process to different substrates. Because the protein's N-terminus is required for the stabilization of APE1 interaction with NPM1 or rRNA and for the control of the overall endonuclease activity (possibly decreasing the rate of product release once in the positively charged state; Fantini *et al.*, 2010; Figure 5), this region-specific multitasking function can provide a "trigger" for molecular regulation with important biological significance. This should be regarded, however, in light of BER coordination to prevent formation of harmful, unprotected DNA strand breaks. Therefore subcellular distribution of APE1 and its enzymatic activity seem to be finely tuned to demand and in a time-dependent manner through multiple interactions with various protein partners and the coordinated occurrence of different PTMs, such as acetylation and ubiquitination (Busso *et al.*, 2009, 2011). The observation that acetylation at $K^{27}/K^{31}/K^{32}/K^{35}$ residues may favor a transition toward a more organized conformation (Supplemental Figure S8) would support the notion that this modification may significantly modulate the interaction with several protein partners on a structural basis. In addition, acetylation at the mentioned K residues may profoundly affect APE1 protein stability, based on a recent report showing that the same K residues can be also polyubiquitinated by UBR3, targeting the protein for degradation by the proteasome (Meisenberg *et al.*, 2011). Given that acetylation competes with ubiquitination for the same K residues, it may represent the switch for controlling protein turnover rate. In this context, the acetylation at these residues that we observed during cell response to genotoxicants may stabilize protein half-life, thus preventing its degradation.

Few studies have reported on the effect of acetylation on the structure of small, ordered (Hughes and Waters, 2006; Liu and Duan, 2008) and disordered (Smet-Nocca *et al.*, 2010) peptides. Molecular dynamic simulations carried out on a peptide from the histone H3 N-terminal tail in the nonacetylated and doubly acetylated forms revealed that acetylation, although not appreciably disturbing the overall structure of the most-populated states, influenced peptide stability (Liu and Duan, 2008). The effect of acetylation at K residues on the conformational properties of small random-coil peptides from the histone H4 N-terminal tail and from nonhistone thymine DNA glycosylase indicated that acetylation had little effect on the

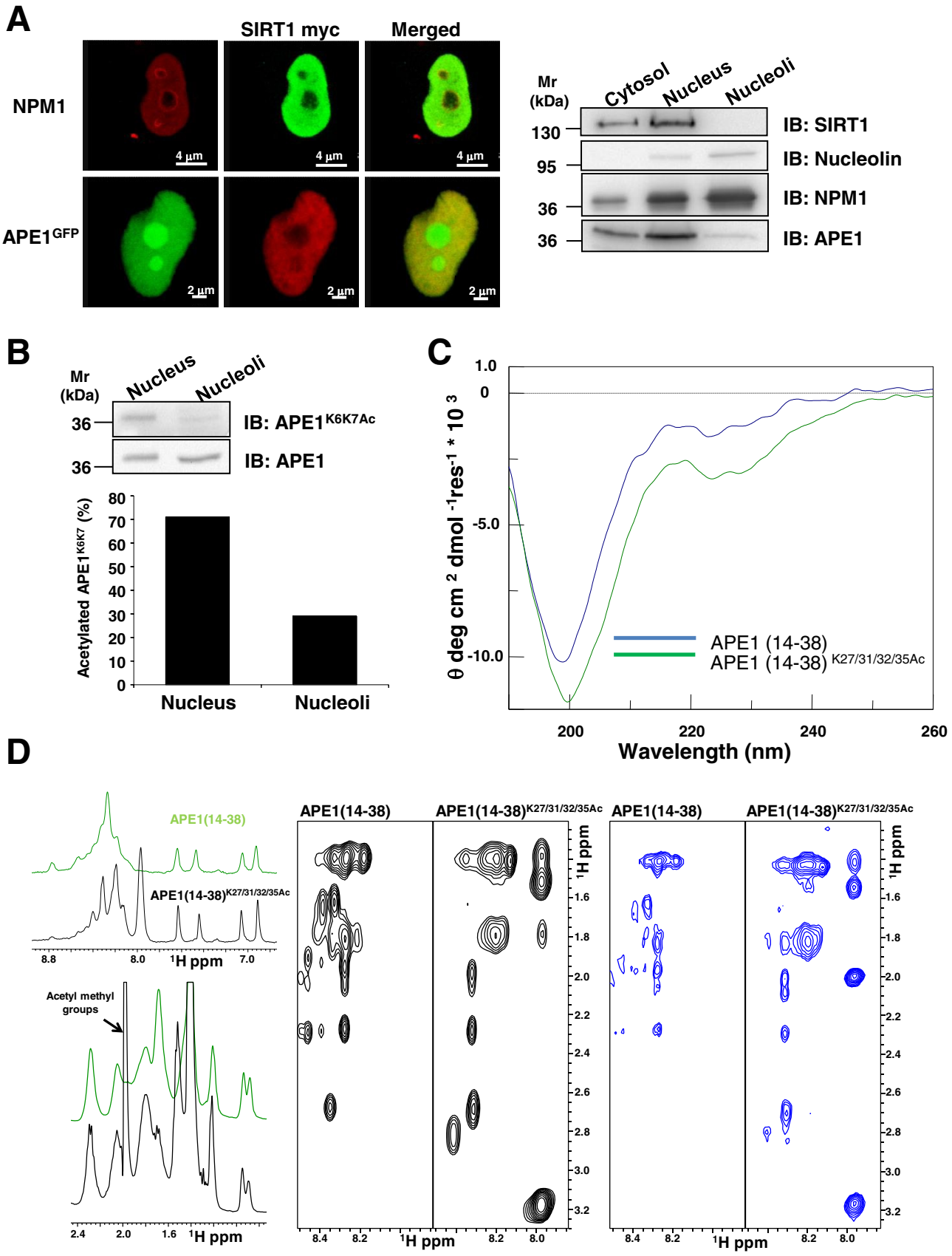

FIGURE 8: Nucleolar APE1 hypoacetylated on K^6/K^7 and conformational impact of acetylation at $K^{27}/K^{31}/K^{32}/K^{35}$ on APE1 local structure. (A) SIRT1 resides within the nucleoplasm of HeLa cells. Left, confocal microscopy of HeLa cells cotransfected with green fluorescent protein–fused APE1 ($APE1^{GFP}$) and c-myc-SIRT1 after fixing and staining with antibodies against NPM1 (red) and c-myc-SIRT1 (top, green; bottom, red). SIRT1, clearly excluded from nucleoli,

overall polypeptide structure, while inducing local conformational changes (Smet-Nocca *et al.*, 2010). In agreement with these studies, APE1(14–38) and APE1(14–38)$^{K27/31/32/35Ac}$ became disordered, as shown by the lack of ROE (Bax and Davis, 1985) cross-peak patterns, which are characteristic of ordered secondary structure elements. However, small differences in the NMR spectra (Figure 8 and Supplemental Figure S8), concerning both chemical shift values and signal intensities, seem to indicate that at least local conformational changes may occur following acetylation. We cannot ignore that these changes may be important for the interaction of APE1 with SIRT1 deacetylase and with NPM1; they highlight the role that the charged status of K residues within this region may play at the protein structural level. Based on our data, it can be speculated that full acetylation of $K^{27–35}$ may reduce SIRT1 binding to APE1, thus delaying its enzymatic activity on K^6/K^7. This mechanism could represent a way to coordinate the kinetics of the overall acetylation status of the protein. According to this hypothesis, SIRT1 should first deacetylate $K^{27–35Ac}$ before deacetylating K^6/K^{7Ac}. Our ability to identify APE1 peptides with varying amounts of acetylation on $K^{27–35}$ supports the existence of a dynamic equilibrium between multiple acetylated forms of the protein within cells and thus its functional regulatory role. Moreover, the presence of SIRT1, found exclusively in the nucleoplasm but not in the nucleoli (similar to the APE1 acetylated on $K^{27–35}$ and the reduced nucleolar presence of APE1 acetylated on K^6/K^7; Figure 8, A and B), suggests that acetylation of APE1 may force its exit from nucleoli to nucleoplasm, where it can be deacetylated by SIRT1. This model is further supported by the significantly reduced interaction of AcAPE1K^{27-35} with NPM1 (Figure 2). Further studies to identify the acetyltransferase able to acetylate APE1 within the nucleoli are in progress. Furthermore, this work supports findings by Yu *et al.* (2010), who demonstrated that these K residue conformational adjustments were concomitant with DNA binding and catalysis or with interaction with Pol β.

The nucleolar role of APE1 storage and regulation, as described here, may have profound biological consequences during cell response to stressor signals, especially in light of recent evidence pointing to the nucleolus as a central hub in DNA damage (Nalabothula *et al.*, 2010). Accordingly, the nucleolus seems responsible for actively transmitting signals to the molecular complex regulating p53 activity mediated by ARF–NPM1 interaction (Colombo *et al.*, 2002; Lee *et al.*, 2005; Nalabothula *et al.*, 2010), and thus it is involved in the maintenance of genome stability. A careful elucidation of the NPM1-ARF-p53 signaling networks and their involvement in the DNA-repair pathway coordinated by APE1 is an important subject for molecular carcinogenesis and deserves further study. This is also underway in our laboratory. Of note, data obtained in this work not only show that nucleoli may act as a storage site so that an appropriate amount of APE1 is readily available for maintenance of genome stability, but also emphasize that nucleolar accumulation of APE1 controls cell proliferation, possibly through its rRNA cleansing function. Compatible with this, APE1^{K4pleA}-expressing cells, under basal conditions, showed impairment in proliferation rate with respect to APE^{WT}-expressing ones (Figure 3). Therefore it can be speculated that nucleolar APE1 is responsible for functional activity of the nucleolus in ribosome biogenesis. APE1 release from the nucleoli after genotoxic treatment may constitute a signal to block active protein synthesis and allow activation of the proper DNA-repair mechanisms. Experiments are in progress along these lines to address this in light of the possibility that acetylation may control the APE1 trafficking from nucleoli to nucleoplasm.

In conclusion, our data shed light on novel molecular aspects highlighting the multifunctional nature of APE1 in regulating different biological outcomes and point to acetylation as an important mechanism for the fine-tuning of protein functions, subcellular distribution, and stability. They also emphasize the need for additional investigation of the APE1 N-terminal domain in order to understand the structural details of the regulatory mechanisms for this multifunctional protein. In addition, recent evidence on APE1 acetylation pattern in triple-negative breast cancer reveals that, concomitantly with total APE1 overexpression, a profound deregulation of APE1 acetylation status occurs under pathological conditions (Poletto *et al.*, 2012). This underscores the biological relevance of our findings and the need for future investigation.

MATERIALS AND METHODS

Inducible APE1 knockdown and generation of APE1 knock-in cell lines

Inducible silencing of endogenous APE1 and reconstitution with mutant proteins in HeLa cell clones was performed as described (Vascotto *et al.*, 2009a,b) and as reported in the Supplemental Information. For inducible shRNA experiments, doxycycline (1 μg/ml; Sigma-Aldrich, St. Louis, MO) was added to the cell culture medium, and cells were grown for 10 d. All biological data were reproduced in at least two different cell clones for each model.

Cell culture and transient transfection with plasmids or siRNA knockdown

HeLa cells were grown in DMEM (Invitrogen, Carlsbad, CA) supplemented with 10% fetal bovine serum (EuroClone, Milan, Italy), 100 U/ml penicillin, and 100 μg/ml streptomycin sulfate. One day

colocalizes with APE1 in the nucleoplasm. The inner part of nucleoli, marked in the granular zone by NPM1, is negative for SIRT1. Right, biochemical isolation of nucleoli confirms that SIRT1 localizes in the nucleoplasmic fraction and it is excluded from nucleoli, where nucleolin, NPM1, and APE1 reside (see *Materials and Methods* for details). Nucleolin was used as a positive control for nuclear and nucleolar compartment. (B) Acetylated K^6/K^7-containing APE1 is enriched within the nucleoplasmic compartment with respect to nucleoli. After normalization for total APE1 protein amount, the levels of acetylated APE1 in nucleolar and nucleoplasmic fractions were analyzed through Western blotting. APE1 acetylated at K^6/K^7 residues is predominately present within the nucleoplasmic fraction, whereas it is reduced in the nucleolar fraction. The histogram indicates the relative percentage amount of acetylated APE1 obtained from the densitometric quantification of acetylated APE1 bands normalized with respect to the amount of total APE1 in each fraction. Each bar represents the mean of two independent experiments whose variation was <10%. (C) CD spectra of the APE1(14–38) and APE1(14–38)$^{K27/31/32/35Ac}$ peptides in 10 mM phosphate buffer, pH 7. (D) Comparison of 1D (left), 2D [^{1}H, ^{1}H] TOCSY (middle), and 2D [^{1}H, ^{1}H] ROESY (right) spectra of APE1(14–38) and APE1(14–38)$^{K27/31/32/35Ac}$ peptides in 10 mM phosphate buffer, pH 7.0. Two different expansions of the proton 1D spectrum are shown; the region between 0.8 and 2.4 ppm, in the lower inset, contains signals from side-chain protons. Acetyl methyl groups originate a peak around 2 ppm, which can be clearly seen in the spectrum of the acetylated peptide; peaks of backbone and side-chain $_N$H atoms appear between 7.0 and 8.8 ppm in the upper inset. For 2D [^{1}H, ^{1}H] TOCSY and 2D [^{1}H, ^{1}H] ROESY experiments the H_N-aliphatic protons correlation region of the spectra are reported.

before transfection, cells were seeded in 10-cm plates at a density of 3.0×10^6 cells/plate. Cells were then transiently transfected with the indicated plasmids using the Lipofectamine 2000 reagent (Invitrogen), according to the manufacturer's instructions. Cells were harvested either 24 or 48 h after transfection, as indicated.

For SIRT1-knockdown experiments, HeLa clones were transfected with 150 nM siRNA siGENOME SMART pool or negative control siRNA 5′-CCAUGAGGUCAUGGUCUGdTdT-3′ (Dharmacon, Lafayette, CO), using Oligofectamine (Invitrogen). After 72 h the cells were harvested.

Preparation of total cell extracts and anti-FLAG coimmunoprecipitation

Preparation of total cell lysates and coimmunoprecipitation analyses were performed as described (Vascotto *et al.*, 2009a,b).

Determination of AP endonuclease activity and abasic site assay

Determination of APE1 AP endonuclease activity was performed using an oligonucleotide cleavage assay, as described previously (Vascotto *et al.*, 2009b) and detailed in the Supplemental Information.

Mass spectrometric analysis of APE1 acetylation

Characterization of APE1 acetylation was performed on the immunopurified protein obtained from APE1-FLAG–expressing HeLa cells (Vascotto *et al.*, 2009b). APE1 was resolved by SDS–PAGE; corresponding protein bands were excised, S-alkylated, and digested with endoprotease AspN (Fantini *et al.*, 2010). Digest aliquots were directly analyzed by nanoLC-ESI-LIT-MS/MS using an LTQ XL mass spectrometer (ThermoFisher Scientific, Waltham, MA) equipped with a Proxeon nanospray source connected to an Easy-nanoLC (ThermoFisher Scientific; Arena *et al.*, 2010; Scippa *et al.*, 2010), and analysis of APE1 acetylation was performed as described (D'Ambrosio *et al.*, 2006) and detailed in the Supplemental Information. A semiquantitative measurement of the amino acid modification was obtained by extracting and integrating nanoLC-ESI-LIT-MS peak areas corresponding to *m/z* values of the modified and nonmodified peptides in the same total ion chromatogram (Salzano *et al.*, 2011). Modification extent was then assayed by evaluating the peak area of the modified peptide with respect to that of the modified peptide plus that of the nonmodified peptide, assuming identical ionization properties for modified and nonmodified species. All these analyses were performed in triplicate.

Antibodies for immunofluorescence and immunoblotting

Antibodies used were anti-NPM1 monoclonal, anti-nucleolin monoclonal (Zymed, Invitrogen), anti-FLAG peroxidase-conjugated, anti-GST peroxidase-conjugated, anti-SIRT1 polyclonal (Abcam, Cambridge, MA), anti–c-myc (Santa Cruz Biotechnology, Santa Cruz, CA), and anti–β-tubulin monoclonal (Sigma-Aldrich). Anti-APE1 monoclonal (Vascotto *et al.*, 2009a) and anti-APE1^{K6K7Ac} (Bhakat *et al.*, 2003) were described previously. Anti-APE1$^{K27\text{-}35Ac}$ polyclonal antibody was generated by PRIMM (Milan, Italy; Poletto *et al.*, 2012).

Western blot analyses

For Western blot analyses, the indicated amounts of cell extracts were resolved in 12% SDS–PAGE and transferred to nitrocellulose membranes (Schleicher & Schuell BioScience, Dassel, Germany). Membranes were blocked with 5% (wt/vol) nonfat dry milk in phosphate-buffered saline (PBS) containing 0.1% (vol/vol) Tween 20 and probed with the indicated antibodies; blots were developed by using the ECL enhanced chemiluminescence procedure (GE Healthcare Piscataway, NJ) or Western Lightning Ultra (PerkinElmer, Waltham, MA). Normalization was performed by using a monoclonal anti-tubulin antibody (Sigma-Aldrich). Blots were quantified by using a Chemidoc XRS video densitometer (Bio-Rad, Hercules, CA).

Plasmids and expression of recombinant proteins

Expression and purification of recombinant proteins from *E. coli* were performed as previously described (Vascotto *et al.*, 2009b; Fantini *et al.*, 2010). Where recombinant proteins were used for in vitro assays, the acronym rAPE1 is used.

GST pull-down assay

A 150-pmol amount of either GST-tagged rAPE1^{WT} or mutant proteins was added to 15 μl of glutathione–Sepharose 4B beads (GE Healthcare), together with equimolar amounts of recombinant NPM1. Binding was performed in PBS, supplemented with 1 mM dithiothreitol (DTT) and 0.5 mM phenylmethylsulfonyl fluoride (PMSF) for 2 h, under rotation, at 4°C. Beads were washed three times with PBS, supplemented with 0.1% (vol/vol) Igepal CA-630 (Sigma-Aldrich), 1 mM DTT, and 0.5 mM PMSF and resuspended in Laemmli sample buffer for Western blot analysis.

DNA–RNA ChIP assays

DNA–RNA ChIP assays were carried out by using a modified version of a protocol described earlier (Gilbert *et al.*, 2000) and as detailed in the Supplemental Information.

Enzymatic fluorescence assays

To examine in vitro deacetylase activity on the acetylated APE1 region 25–38, we used the SIRT Fluorescent Activity Assay Kit (Biomol, Plymouth, PA). Optimizing manufacturer's instructions, we used white plates (OPTI PLATE; PerkinElmer) with 384 wells at reduced volume (total reaction volume, 20 μl). Purified peptides were incubated in 25 mM Tris-HCl, pH 8.0, 2.7 mM KCl, 137 mM NaCl, 1 mM $MgCl_2$, and 1 mg/ml bovine serum albumin containing the enzyme (0.04 U/μl) and 25 μM Fluor de Lys-p53 peptide substrate (Arg-His-Lys-Lys [Ac], from region 379–382 of human p53) in the presence/absence of 250 μM NAD^+ for 30 min at 37°C. Deacetylase activity was measured in arbitrary fluorescence units at 460 nm. Dose–response experiments were carried out by using a 0–500 μM range of peptide concentration. Data fitting was performed using the GraphPad Prism 4 software, version 4.02 (GraphPad, La Jolla, CA). Data were in triplicate/duplicate from three independent assays.

Immunofluorescence confocal and proximity ligation analyses

Immunofluorescence procedures and PLA were carried out as described earlier (Vascotto *et al.*, 2009b, 2011). To study the interaction between APE1 and NPM1 in vivo, we used the in situ Proximity Ligation Assay technology (Olink Bioscience, Uppsala, Sweden). After incubation with monoclonal anti-APE1 (1:50) or anti-FLAG antibody (1:200) for 3 h at 37°C, cells were incubated with polyclonal anti-NPM1 (1:200) overnight at 4°C. PLA was performed following manufacturer's instructions. Technical controls, represented by the omission of anti-NPM1 primary antibody, resulted in the complete loss of PLA signal. Cells were visualized through a Leica TCS SP laser-scanning confocal microscope (Leica Microsystems, Wetzlar, Germany). Determination of PLA signals was performed using BlobFinder software (Center for Image Analysis, Uppsala University, Uppsala, Sweden). PLA technology was also used to detect acetylated APE1 at $K^{27}/K^{31}/K^{32}/K^{35}$ residues. Cells were incubated with the

anti-APE1$^{K27–35Ac}$ rabbit-polyclonal antibody diluted 1:1500 and then with a mouse-monoclonal anti-APE1 antibody (1:27). PLA was subsequently carried out following manufacturer's instructions.

Confocal analyses of APE1-Dendra fusion protein through in vivo live imaging

For in vivo APE1-Dendra trafficking studies, HeLa cells were seated on glass-bottom Petri dishes (thickness #1.5; WillCo Wells, Amsterdam, Netherlands), transfected with APE1-Dendra constructs, and grown in the presence of DMEM without phenol red. A Leica TCS SP laser-scanning confocal microscope was equipped with a heating system (Incubator S) and a CO_2 controller (CTI Controller 3700 digital) to maintain cells in optimal growing conditions. Images were captured 24 h after transfection using a 63× oil fluorescence objective. For Dendra green fluorescence acquisition a 488-nm argon laser was regulated at 10% of power with PTM 750 V.

Cell viability, cell growth, and clonogenic assays

Cell viability was measured by using the MTS assay (Celltiter 96 Aqueous One solution cell proliferation assay; Promega, Madison, WI) on HeLa cells stably expressing APE1^{WT}, APE1^{K4pleA}, and APE1^{K4pleR} proteins grown in 96-well plates. After MMS (Sigma-Aldrich) treatment or TBHP (Sigma-Aldrich), the MTS solution was added to each well and the plates were incubated for 2 h. Absorbance was measured at 490 nm by using a multiwell plate reader. The values were standardized to wells containing media alone.

Cell growth assays were performed as described (Vascotto *et al.*, 2009a,b) and detailed in the Supplemental Information, and clonogenic assays were performed according to Plumb (1999) and essentially as described previously (Vascotto *et al.*, 2009a,b).

Circular dichroism spectroscopy

CD spectra were recorded on a Jasco J-810 spectropolarimeter (Jasco, Tokyo, Japan) at 25°C in the far-UV region from 190 to 260 nm. Each spectrum was obtained by averaging three scans, subtracting contributions from the corresponding blanks, and converting the signal to mean residue ellipticity in units of deg-cm^2 dmol^{-1} res^{-1}. Other experimental settings were 20 nm/min scan speed, 2.0 nm bandwidth, 0.2 nm resolution, 50 mdeg sensitivity, and 4 s response. Peptide concentration was kept at 100 μM, and a 0.1 cm path-length quartz cuvette was used. Spectra were acquired in 10 mM phosphate buffer, pH 7.0, containing various percentages of TFE.

NMR spectroscopy

NMR samples were prepared by dissolving APE1 peptides (1.5–2 mg) either in 600 μl of a 10 mM phosphate buffer, pH 7, containing 10% (vol/vol) D_2O or in a mixture of 10 mM phosphate buffer:2-2-2 trifluorethanol-d3 (98% deuterium; Armar Chemicals, Döttingen, Switzerland) 70:30 (vol/vol). The 2D [^{1}H, ^{1}H] TOCSY spectra (1024 × 256 total data points, 32 scans per t1 increment, 70 ms mixing time; Griesinger *et al.*, 1988) were recorded at 298 K on a Varian ^{UNITY}INOVA 600 spectrometer (Palo Alto, CA) equipped with a cold-probe. The 1D proton (128 scans and a relaxation delay of 1.5 s) and 2D [^{1}H, ^{1}H] ROESY (2048 × 256 total data points, 64 scans per t1 increment, 200 ms mixing time) spectra were acquired at 298 K on a Varian ^{UNITY}INOVA 400 spectrometer provided with *z*-axis pulsed-field gradients and a triple-resonance probe. Water signal was suppressed by means of either double pulsed field gradient selective echo techniques (Dalvit, 1998) or continuous wave irradiation. Varian software VNMRJ 1.1D was implemented for spectral processing. The programs MestRe-C2.3a (Universidade de Santiago de Compostela, Santiago de Compostela, Spain) and NEASY (Bartels *et al.*, 1995; www.nmr.ch) were used for analysis of 1D and 2D NMR data, respectively.

Statistical analyses

Statistical analyses were performed by using the Excel (Microsoft, Redmond, WA) data analysis program for Student's *t* test. $p < 0.05$ was considered as statistically significant.

ACKNOWLEDGMENTS

We thank Paolo Peruzzo for generation of mutant recombinant proteins, K. Irani for providing SIRT1-encoding plasmids, and Pablo Radicella for helpful comments on the manuscript. We also thank Julie Driscol for excellent help in editing the manuscript. This work was supported by the Associazione Italiana per la Ricerca sul Cancro (IG10269) and the Ministero dell'Istruzione, dell'Università e della Ricerca (FIRB_RBRN07BMCT and PRIN2008_CCPKRP_003 to G.T.; PRIN2008_CCPKRP_002 and FIRB2008_RBNE08YFN3_003 to A.S.). This work was also supported by a UICC Yamagiwa-Yoshida Memorial International Cancer Study Grant to G.T. and by the Regione Friulia Venezia Giulia for the Project MINA under the Programma per la Cooperazione Transfrontaliera Italia-Slovenia 2007–2013.

REFERENCES

Arena S, Renzone G, Novi G, Paffetti A, Bernardini G, Santucci A, Scaloni A (2010). Modern proteomic methodologies for the characterization of lactosylation protein targets in milk. Proteomics 10, 3414–3434.

Bapat A, Fishel ML, Kelley MR (2009). Going Ape as an approach to cancer therapeutics. Antioxid Redox Signal 11, 651–668.

Bapat A, Glass LS, Luo M, Fishel ML, Long EC, Georgiadis MM, Kelley MR (2010). Novel small-molecule inhibitor of apurinic/apyrimidinic endonuclease 1 blocks proliferation and reduces viability of glioblastoma cells. J Pharmacol Exp Ther 334, 988–998.

Barnes T, Kim WC, Mantha AK, Kim SE, Izumi T, Mitra S, Lee CH (2009). Identification of apurinic/apyrimidinic endonuclease 1 (APE1) as the endoribonuclease that cleaves c-myc mRNA. Nucleic Acids Res 37, 3946–3958.

Bartels C, Xia T, Billeter M, Gunthert P, Wüthrich K (1995). The program XEASY for computer-supported NMR spectral analysis of biological macromolecules. J Biomol NMR 6, 1–10.

Bax A, Davis DG (1985). Practical aspects of two-dimensional transverse NOE spectroscopy. J Magn Reson 63, 207–213.

Bhakat KK, Izumi T, Yang SH, Hazra TK, Mitra S (2003). Role of acetylated human AP-endonuclease (APE1/Ref-1) in regulation of the parathyroid hormone gene. EMBO J 1, 6299–6309.

Busso CS, Iwakuma T, Izumi T (2009). Ubiquitination of mammalian AP endonuclease (APE1) regulated by the p53-MDM2 signaling pathway. Oncogene 28, 1616–1625.

Busso CS, Wedgeworth CM, Izumi T (2011). Ubiquitination of human AP-endonuclease 1 (APE1) enhanced by T233E substitution and by CDK5. Nucleic Acids Res 39, 8017–8028.

Chattopadhyay R, Wiederhold L, Szczesny B, Boldogh I, Hazra TK, Izumi T, Mitra S (2006). Identification and characterization of mitochondrial abasic (AP)-endonuclease in mammalian cells. Nucleic Acids Res 34, 2067–2076.

Chudakov DM, Lukyanov S, Lukyanov KA (2007). Tracking intracellular protein movements using photoswitchable fluorescent protein PS-CFP2 and Dendra2. Nat Protoc 2, 2024–2032.

Colombo E, Marine JC, Danovi D, Falini B, Pelicci PG (2002). Nucleophosmin regulates the stability and transcriptional activity of p53. Nat Cell Biol 4, 529–533.

Dalvit C (1998). Efficient multiple-solvent suppression for the study of the interaction of organic solvents with biomolecules. J Biomol NMR 11, 437–444.

D'Ambrosio C, Arena S, Fulcoli G, Scheinfeld MH, Zhou D, D'Adamio L, Scaloni A (2006). Hyperphosphorylation of JNK-interacting protein 1, a protein associated with Alzheimer disease. Mol Cell Proteomics 5, 97–113.

Demple B, DeMott MS (2002). Dynamics and diversions in base excision DNA repair of oxidized abasic lesions. Oncogene 21, 8926–8934.

Fantini D *et al.* (2008). APE1/Ref-1 regulates PTEN expression mediated by Egr1. Free Radic Res 42, 20–29.

Fantini D *et al*. (2010). Critical lysine residues within the overlooked N-terminal domain of human APE1 regulate its biological functions. Nucleic Acids Res 38, 8239–8256.
Fung H, Demple B (2005). A vital role for APE1/Ref1 protein in repairing spontaneous DNA damage in human cells. Mol Cell 17, 463–470.
Garbutt GJ, Abraham EC (1981). Non-enzymatic acetylation of human hemoglobins. Biochim Biophys Acta 670, 190–194.
Gilbert SL, Pehrson JR, Sharp PA (2000). XIST RNA associates with specific regions of the inactive X chromatin. J Biol Chem 275, 36491–36494.
Gray MJ, Zhang J, Ellis LM, Semenza GL, Evans DB, Watowich SS, Gallick GE (2005). HIF-1alpha, STAT3, CBP/p300 and Ref-1/APE are components of a transcriptional complex that regulates Src-dependent hypoxia-induced expression of VEGF in pancreatic and prostate carcinomas. Oncogene 24, 3110–3120.
Griesinger C, Otting G, Wüthrich K, Ernst RR (1988). Clean TOCSY for 1H spin system identification in macromolecules. J Am Chem Soc 110, 7870–7872.
Grillo C, D'Ambrosio C, Scaloni A, Maceroni M, Merluzzi S, Turano C, Altieri F (2006). Cooperative activity of Ref-1/APE and ERp57 in reductive activation of transcription factors. Free Radic Biol Med 41, 1113–1123.
Hirota K, Matsui M, Iwata Z, Nishiyama A, Mori K, Yodoi J (1997). AP-1 transcriptional activity is regulated by a direct association between thioredoxin and Ref-1. Proc Natl Acad Sci USA 94, 3633–3638.
Hughes RM, (2006). Effects of lysine acetylation in a beta-hairpin peptide: comparison of an amide-pi and a cation-pi interaction. J Am Chem Soc 128, 13586–13591.
Izumi T, Brown DB, Naidu CV, Bhakat KK, Macinnes V, Saito H, Chen DJ, Mitra S (2005). Two essential but distinct functions of the mammalian abasic endonuclease. Proc Natl Acad Sci USA 102, 5739–5743.
Lazzé MC, Pizzala R, Savio M, Stivala LA, Prosperi E, Bianchi L (2003). Anthocyanins protect against DNA damage induced by tert-butyl-hydroperoxide in rat smooth muscle and hepatoma cells. Mutat Res 535, 103–115.
Lee C, Smith BA, Bandyopadhway K, Gjerset RA (2005). DNA damage disrupts the p14ARF-B23(nucleophosmin) interaction and triggers a transient subnuclear redistribution of p14ARF. Cancer Res 65, 9834–9842.
Li M, Vascotto C, Xu S, Dai N, Qing Y, Zhong Z, Tell G, Wang D (2012). Human AP endonuclease/redox factor APE1/ref-1modulates mitochondrial function after oxidative stress by regulating the transcriptional activity of NRF1. Free Radic Biol Med 53, 237–248.
Liu H, Duan Y (2008). Effects of posttranslational modifications on the structure and dynamics of histone H3 N-terminal Peptide. Biophys J 94, 4579–4585.
Marcotte PA, Richardson PL, Guo J, Barrett LW, Xu N, Gunasekera A, Glaser KB (2004). Fluorescence assay of SIRT protein deacetylases using an acetylated peptide substrate and a secondary trypsin reaction. Anal Biochem 332, 90–99.
Meisenberg C *et al*. (2011). Ubiquitin ligase UBR3 regulates cellular levels of the essential DNA repair protein APE1 and is required for genome stability. Nucleic Acids Res 40, 701–711.
Mitra S, Izumi T, Boldogh I, Bhakat KK, Chattopadhyay R, Szczesny B (2007). Intracellular trafficking and regulation of mammalian AP-endonuclease 1 (APE1), an essential DNA repair protein. DNA Repair 6, 461–469.
Nalabothula N, Indig FE, Carrier F (2010). The nucleolus takes control of protein trafficking under cellular stress. Mol Cell Pharmacol 2, 203–212.
Parlanti E, Locatelli G, Maga G, Dogliotti E (2007). Human base excision repair complex is physically associated to DNA replication and cell cycle regulatory proteins. Nucleic Acids Res 35, 1569–1577.
Parsons JL, Tait PS, Finch D, Dianova II, Allinson SL, Dianov GL (2008). CHIP-mediated degradation and DNA damage-dependent stabilization regulate base excision repair proteins. Mol Cell 29, 477–487.
Pines A, Bivi N, Romanello M, Damante G, Kelley MR, Adamson ED, D'Andrea P, Quadrifoglio F, Moro L, Tell G (2005). Cross-regulation between Egr-1 and APE/Ref-1 during early response to oxidative stress in the human osteoblastic HOBIT cell line: evidence for an autoregulatory loop. Free Radic Res 39, 269–281.
Poletto M, Loreto CD, Marasco D, Poletto E, Puglisi F, Damante G, Tell G (2012). Acetylation on critical lysine residues of apurinic/apyrimidinic endonuclease 1 (APE1) in triple negative breast cancers. Biochem Biophys Res Commun 424, 34–39.
Plumb JA (1999). Cell sensitivity assays: clonogenic assay. Methods Mol 28, 17–23.
Salzano AM, Renzone G, Scaloni A, Torreggiani A, Ferreri C, Chatgilialoglu C (2011). Human serum albumin modifications associated with reductive radical stress. Mol Biosyst 7, 889–898.
Schnell U, Dijk F, Sjollema KA, Giepmans BN (2012). Immunolabeling artifacts and the need for live-cell imaging. Nat Methods 9, 152–158.
Scippa GS, Rocco M, Ialicicco M, Trupiano D, Viscosi V, Di Michele M, Arena S, Chiatante D, Scaloni A (2010). The proteome of lentil (*Lens culinaris* Medik.) seeds: discriminating between landraces. Electrophoresis 31, 497–506.
Seemann S, Hainaut P (2005). Roles of thioredoxin reductase 1 and APE/Ref-1 in the control of basal p53 stability and activity. Oncogene 24, 3853–3863.
Sengupta S, Mantha AK, Mitra S, Bhakat KK (2011). Human AP endonuclease (APE1/Ref-1) and its acetylation regulate YB-1-p300 recruitment and RNA polymerase II loading in the drug-induced activation of multidrug resistance gene MDR1. Oncogene 30, 482–493.
Smet-Nocca C, Wieruszeski JM, Melnyk O, Benecke A (2010). NMR-based detection of acetylation sites in peptides. J Pept Sci 16, 414–423.
Szczesny B, Mitra S (2005). Effect of aging on intracellular distribution of abasic (AP) endonuclease 1 in the mouse liver. Mech Ageing Dev 126, 1071–1078.
Tell G, Crivellato E, Pines A, Paron I, Pucillo C, Manzini G, Bandiera A, Kelley MR, Di Loreto C, Damante G (2001). Mitochondrial localization of APE/Ref-1 in thyroid cells. Mutat Res 485, 143–152.
Tell G, Damante G, Caldwell D, Kelley MR (2005). The intracellular localization of APE1/Ref-1: more than a passive phenomenon. Antioxid Redox Signal 7, 367–384.
Tell G, Fantini D, Quadrifoglio F (2010a). Understanding different functions of mammalian AP endonuclease (APE1) as a promising tool for cancer treatment. Cell Mol Life Sci 67, 3589–3608.
Tell G, Quadrifoglio F, Tiribelli C, Kelley MR (2009). The many functions of APE1/Ref-1: not only a DNA-repair enzyme. Antioxid Redox Signal 11, 601–620.
Tell G, Wilson DM 3rd (2010). Targeting DNA repair proteins for cancer treatment. Cell Mol Life Sci 67, 3569–3572.
Tell G, Wilson DM 3rd, Lee CH (2010b). Intrusion of a DNA repair protein in the RNome world: is this the beginning of a new era. Mol Cell Biol 30, 366–371.
Ueno M, Masutani H, Arai RJ, Yamauchi A, Hirota K, Sakai T, Inamoto T, Yamaoka Y, Yodoi J, Nikaido T (1999). Thioredoxin-dependent redox regulation of p53-mediated p21 activation. J Biol Chem 274, 35809–35815.
Vascotto C *et al*. (2011). Knock-in reconstitution studies reveal an unexpected role of Cys-65 in regulating APE1/Ref-1 subcellular trafficking and function. Mol Biol Cell 22, 3887–3901.
Vascotto C *et al*. (2009a). Genome-wide analysis and proteomic studies reveal APE1/Ref-1 multifunctional role in mammalian cells. Proteomics 9, 1058–1074.
Vascotto C *et al*. (2009b). APE1/Ref-1 interacts with NPM1 within nucleoli and plays a role in the rRNA quality control process. Mol Cell Biol 29, 1834–1854.
Vidal AE, Boiteux S, Hickson ID, Radicella JP (2001). XRCC1 coordinates the initial and late stages of DNA abasic site repair through protein-protein interactions. EMBO J 20, 6530–6539.
Wei SJ, Botero A, Hirota K, Bradbury CM, Markovina S, Laszlo A, Spitz DR, Goswami PC, Yodoi J, Gius D (2000). Thioredoxin nuclear translocation and interaction with redox factor-1 activates the activator protein-1 transcription factor in response to ionizing radiation. Cancer Res 60, 6688–6695.
Weibrecht I, Leuchowius KJ, Clausson CM, Conze T, Jarvius M, Howell WM, Kamali-Moghaddam M, Söderberg O (2010). Proximity ligation assays: a recent addition to the proteomics toolbox. Expert Rev Proteomics 7, 401–409.
Wilson DM 3rd, (2010). Small molecule inhibitors of DNA repair nuclease activities of APE1. Cell Mol Life Sci 67, 3621–3631.
Wong HK, Muftuoglu M, Beck G, Imam SZ, Bohr VA, Wilson DM 3rd (2007). Cockayne syndrome B protein stimulates apurinic endonuclease 1 activity and protects against agents that introduce base excision repair intermediates. Nucleic Acids Res 35, 4103–4113.
Yacoub A, Kelley MR, Deutsch WA (1997). The DNA repair activity of human redox/repair protein APE/Ref-1 is inactivated by phosphorylation. Cancer Res 57, 5457–5459.
Yamamori T, DeRicco J, Naqvi A, Hoffman TA, Mattagajasingh I, Kasuno K, Jung SB, Kim CS, Irani K (2010). SIRT1 deacetylates APE1 and regulates cellular base excision repair. Nucleic Acids Res 38, 832–845.
Yu E, Gaucher SP, Hadi MZ (2010). Probing conformational changes in Ape1 during the progression of base excision repair. Biochemistry 49, 3786–3796.
Ziel KA, Campbell CC, Wilson GL, Gillespie MN (2004). Ref-1/Ape is critical for formation of the hypoxia-inducible transcriptional complex on the hypoxic response element of the rat pulmonary artery endothelial cell VEGF gene. FASEB J 18, 986–988.